Mutation of SIMPLE in Charcot–Marie–Tooth 1C alters production of exosomes

Hong Zhu[a,*], Sara Guariglia[b,*], Raymond Y. L. Yu[a], Wenjing Li[a], Deborah Brancho[a], Hector Peinado[c], David Lyden[c], James Salzer[d], Craig Bennett[e], and Chi-Wing Chow[a]

[a]Department of Molecular Pharmacology, Albert Einstein College of Medicine, New York, NY 10461; [b]Program in Neuroscience, CUNY College of Staten Island, New York, NY 10314; [c]Department of Pediatrics, Cell and Developmental Biology, Weill Cornell Medical College, New York, NY 10021; [d]Smilow Neuroscience Program, New York University Langone Medical Center, New York, NY 10016; [e]Division of Genetics and Developmental Medicine, Department of Pediatrics, University of Washington School of Medicine, Seattle, WA 98195

ABSTRACT **Charcot–Marie–Tooth (CMT) disease is an inherited neurological disorder. Mutations in the small integral membrane protein of the lysosome/late endosome (SIMPLE) account for the rare autosomal-dominant demyelination in CMT1C patients. Understanding the molecular basis of CMT1C pathogenesis is impeded, in part, by perplexity about the role of SIMPLE, which is expressed in multiple cell types. Here we show that SIMPLE resides within the intraluminal vesicles of multivesicular bodies (MVBs) and inside exosomes, which are nanovesicles secreted extracellularly. Targeting of SIMPLE to exosomes is modulated by positive and negative regulatory motifs. We also find that expression of SIMPLE increases the number of exosomes and secretion of exosome proteins. We engineer a point mutation on the SIMPLE allele and generate a physiological mouse model that expresses CMT1C-mutated SIMPLE at the endogenous level. We find that CMT1C mouse primary embryonic fibroblasts show decreased number of exosomes and reduced secretion of exosome proteins, in part due to improper formation of MVBs. CMT1C patient B cells and CMT1C mouse primary Schwann cells show similar defects. Together the data indicate that SIMPLE regulates the production of exosomes by modulating the formation of MVBs. Dysregulated endosomal trafficking and changes in the landscape of exosome-mediated intercellular communications may place an overwhelming burden on the nervous system and account for CMT1C molecular pathogenesis.**

Monitoring Editor
Patrick J. Brennwald
University of North Carolina

Received: Jul 24, 2012
Revised: Mar 19, 2013
Accepted: Apr 1, 2013

INTRODUCTION

Charcot–Marie–Tooth (CMT) disease is a common inherited neurological disorder of the peripheral nervous system (Boerkoel *et al.*, 2002; Shy, 2004). CMT1C is a subclass of the CMT1 demyelinating family (Latour *et al.*, 2006; Szigeti and Lupski, 2009). Although CMT1C is a rare form of neuropathy, its distinctive autosomal-dominant trait is unique among the CMT1 family of diseases, as other forms of CMT1 are mainly recessive in nature and affect the level of myelin expression. Mutations in the small integral membrane protein of the lysosome/late endosome (SIMPLE; also known as LITAF, EET1, and PIG7; Myokai *et al.*, 1999; Zhu *et al.*, 1999; Moriwaki *et al.*, 2001; Xie *et al.*, 2002) account for the demyelination found in CMT1C patients (Street *et al.*, 2003; Bennett *et al.*, 2004; Saifi *et al.*, 2005; Latour *et al.*, 2006; Gerding *et al.*, 2009). The molecular basis of these SIMPLE mutations in causing autosomal-dominant demyelination in CMT1C, however, is elusive.

The lack of knowledge on the role of SIMPLE further complicates the understanding of SIMPLE in CMT1C demyelination. Despite the proposal of SIMPLE as a transcription factor (Myokai *et al.*, 1999; Bolcato-Bellemin *et al.*, 2004; Tang *et al.*, 2005), a transcriptional

This article was published online ahead of print in MBoC in Press (http://www.molbiolcell.org/cgi/doi/10.1091/mbc.E12-07-0544) on April 10, 2013.

*These authors contributed equally to this study.

Address correspondence to: Chi-Wing Chow (chi-wing.chow@einstein.yu.edu).

Abbreviations used: CMT, Charcot–Marie–Tooth; ESCRT, endosomal sorting complex required for transport; LactC2, C2 phosphatidylserine-binding domain of lactadherin; MEF, mouse embryonic fibroblast; MVB, multivesicular body; SIMPLE, small integral membrane protein of the lysosome/late endosome.

capability of SIMPLE has not been reproduced (Moriwaki *et al.*, 2001; Huang and Bennett, 2007; Lee *et al.*, 2011; and data not shown). Indeed, punctated localization of SIMPLE in cells implies a role in endosomal regulation and vesicular trafficking.

Vesicular trafficking is a fundamental cellular process that functions to facilitate cargo entry, export, and intracellular transport in cells (Bonifacino and Traub, 2003; Morita and Sundquist, 2004; Haglund and Dikic, 2005; Hurley and Emr, 2006; Slagsvold *et al.*, 2006; van Niel *et al.*, 2006; Piper and Katzmann, 2007). Cargoes are routed to and from the plasma membrane, endoplasmic reticulum, Golgi, and endosomal/lysosomal system for recycling, degradation, and/or export. Endosomal membrane invagination, which is mediated by multiprotein endosomal sorting complex required for transport (ESCRT) complexes (Hurley and Emr, 2006; Hurley, 2010; Hurley *et al.*, 2011; Falguières *et al.*, 2009; Saksena and Emr, 2009; Stuffers *et al.*, 2009; Henne *et al.*, 2011), further generates intraluminal vesicles inside multivesicular bodies (MVBs). Intraluminal vesicles can be released extracellularly as exosomes, for intercellular communications, upon fusion of MVBs with the plasma membrane.

Exosomes are extracellular fractions that contain 40- to 100-nm nanovesicles with specific density of ~1.1–1.2 g/cm^3 (Simons and Raposo, 2009; Huotari and Helenius, 2011). A major hallmark of exosome function is presentation of antigens (Schartz *et al.*, 2002; Chaput *et al.*, 2006; Li *et al.*, 2006; Giri and Schorey, 2008). Another proposed function of secreted exosomes is cell–cell communications via autocrine/paracrine regulation (Trojan horse model; Chaput *et al.*, 2006; Mignot *et al.*, 2006). Indeed, proteomic studies revealed diverse protein cargoes in exosomes, which are secreted in a cell type–specific manner (Aoki *et al.*, 2007; Kramer-Albers *et al.*, 2007; Simpson *et al.*, 2008; Giri *et al.*, 2010). The exosome pathway also participates in viral budding and delivery of mitogens (Aoki *et al.*, 2007; Fang *et al.*, 2007). RNA messages and microRNA are also found in exosomes to mediate exchange of genetic materials (Mathivanan and Simpson, 2009; Mittelbrunn *et al.*, 2011). Thus understanding the molecular machinery of vesicular trafficking will cast new light onto this important biological process.

The purpose of this study is to elucidate the role of SIMPLE and its molecular pathology in CMT1C. We report that SIMPLE resides within the intraluminal vesicles of MVBs and inside exosomes. We show that SIMPLE increases the production of exosomes, whereas CMT1C mutation causes improper formation of MVBs, accumulation of lysosomes, and reduced secretion of exosomes. We propose that SIMPLE is a previously unrecognized player in regulating the production of exosomes. Elevated intracellular stress or ineffective extracellular communications could account for the pathological consequences of CMT1C mutation.

RESULTS

Intracellular locations of SIMPLE

Previous studies indicated localization of SIMPLE in endosomal trafficking compartments (Moriwaki *et al.*, 2001; Eaton *et al.*, 2011; Lee *et al.*, 2011). Indeed, signature motifs for endocytic functions, including di-Leu (LL) and YKRL motifs, are found on SIMPLE (Figure 1A). In addition, SIMPLE encodes a PTAP motif for binding of ESCRT1 protein Tsg101 (Saifi *et al.*, 2005; Shirk *et al.*, 2005), a key component of multiprotein ESCRT complexes for the formation of MVBs (Falguières *et al.*, 2009; Hurley, 2010; Henne *et al.*, 2011; Rusten *et al.*, 2012). SIMPLE also encodes PPxY motifs for binding of Nedd4 type E3 ubiquitin ligases (Jolliffe *et al.*, 2000; Shirk *et al.*, 2005; Eaton *et al.*, 2011), key regulatory molecules in ubiquitin-mediated signaling and viral budding (Timmins *et al.*, 2003; Chen and Matesic, 2007; Zwang and Yarden, 2009; Hurley and Hanson, 2010; Rauch and Martin-Serrano, 2011). Thus we first ascertained localization of exogenous SIMPLE in transfected cells and found, as reported (Moriwaki *et al.*, 2001; Eaton *et al.*, 2011; Lee *et al.*, 2011), punctated staining pattern with partial colocalization of SIMPLE with LAMP2 and Rab7 in lysosomes and late endosomes, respectively (Figure 1, B and C). Among the punctated staining pattern, we also found partial colocalization of SIMPLE and lysobisphosphatidic acid (LBPA), a specific lipid present in late endosomes/MVBs (Figure 1D). Minimal colocalizations in the punctae, however, were detected by SIMPLE and early endosome antigen-1 (EEA1) (Figure 1E). Taken together, these data indicate that SIMPLE is present in late endosomes/MVBs and lysosomes.

We further performed immuno–electron microscopy to establish the intracellular localization of SIMPLE. As expected, SIMPLE was found in endosome-like tubular structures and lysosome-like, electron-dense granules (Figure 1F). Surprisingly, we also found membrane-bound SIMPLE on intraluminal vesicles inside MVBs (Figure 1F). These data confirm that SIMPLE is present in late endosomes and lysosomes. Unexpectedly, SIMPLE is also localized in intraluminal vesicles inside MVBs.

Localization of SIMPLE inside exosomes

Recent studies indicated that, upon fusion with plasma membrane, intraluminal vesicles inside MVBs can be secreted extracellularly as exosomes (Simons and Raposo, 2009; Huotari and Helenius, 2011). Exosomes, however, are different from microvesicles, which are budded directly from the plasma membranes. Given that SIMPLE localizes in intraluminal vesicles of MVBs, we hypothesized that SIMPLE is secreted via the exosome pathway. To test this hypothesis, we performed differential ultracentrifugation on conditioned media to prepare exosome fractions for detection of endogenous SIMPLE. Conditioned media from NIH 3T3 mouse fibroblasts and primary mouse Schwann cells were examined (Figure 2A). We found that endogenous SIMPLE was present in pelleted exosome fraction, but not in the supernatant, after ultracentrifugation at 100,000 × *g* (Figure 2A). We also confirmed that flotillin, previously detected in exosomes (de Gassart *et al.*, 2003), was present in pelleted exosome fraction after ultracentrifugation at 100,000 × *g* (Figure 2A). Because SIMPLE is widely expressed, we also detected SIMPLE in exosomes in rat primary Schwann cells, HepG2 liver carcinoma cells, MCF7 breast epithelial cancer cells, and COS monkey kidney cells (data not shown). Similarly, exogenously expressed SIMPLE (tagged with either FLAG or hemagglutinin [HA] epitope) and SIMPLE fused to enhanced green fluorescent protein (EGFP) were also targeted to exosomes (Figure 2B), whereas EGFP alone was mainly found in the remaining supernatant after ultracentrifugation at 100,000 × *g* (data not shown). These data indicate that SIMPLE is secreted in exosomes in multiple different cell types.

We further performed sucrose gradient floatation assays to isolate exosomes based on their density (Figure 2C). Sucrose gradient floatation assays indicated that endogenous SIMPLE was enriched in density ~1.13 g/cm^3, within the biochemical characteristic of exosomes (Figure 2C). In addition, Alix, CD63 (LAMP3), and flotillin-1, previously known proteins secreted in exosomes (de Gassart *et al.*, 2003), were also copurified with SIMPLE at the specific density of exosome fractions (Figure 2C). More important, immuno–electron microscopy indicated that SIMPLE was associated with purified exosomes (Figure 2D). These data indicate that SIMPLE is membrane bound and secreted in exosomes.

Our ultrastructural analysis indicated that SIMPLE seems to be localized inside the intraluminal vesicles (Figure 1F). If so, SIMPLE would be protected and encircled inside secreted exosomes. To test

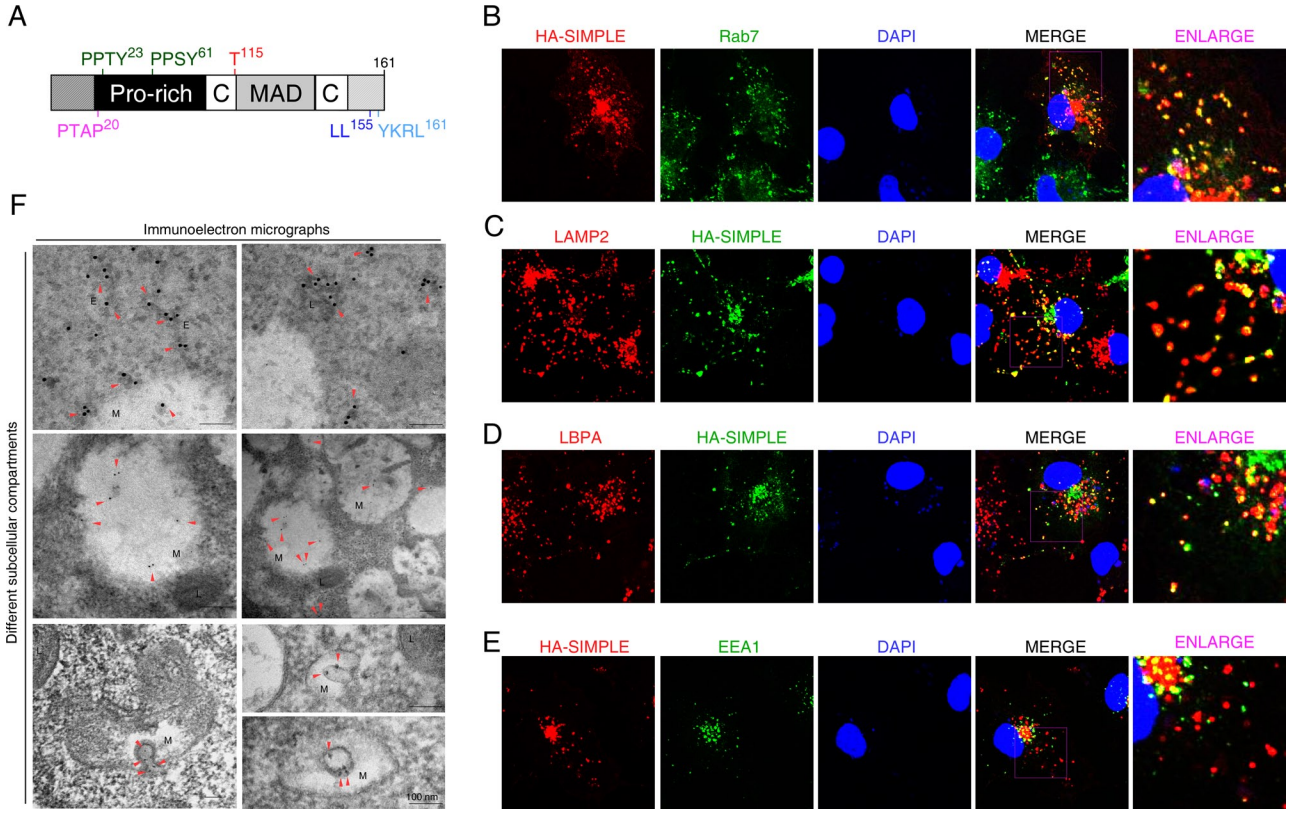

FIGURE 1: Intracellular locations of SIMPLE. (A) Schematic illustration of SIMPLE. Critical motifs known for regulating endosomal trafficking are shown, as is the T115N CMT1C mutation. (B–E) COS cells were transiently transfected with HA-SIMPLE. Confocal microscopy was performed, and cells were costained for exogenous SIMPLE and endogenous Rab7 (B), LAMP2 (C), LBPA (D), and EEA1 (E). DNA in nuclei was visualized using 4′,6-diamidino-2-phenylindole (DAPI; blue). (F) Immuno–electron microscopy was performed to determine the localization of HA-SIMPLE (arrowheads) in transfected COS cells. Endosome-like tubular structures (E), lysosome-like electron-dense granules (L), and multivesicular bodies (M) are shown. Scale bar, 100 nm.

this possibility, we performed immunoprecipitation assays (Figure 2E). Purified exosomes were immunoprecipitated in either lysis buffer to disrupt exosomes or in phosphate-buffered saline (PBS) to keep exosomes intact. Immunoprecipitation assays indicated that SIMPLE could only be immunoprecipitated after lysis (Figure 2E). We further performed limited trypsin digestion on purified exosomes to ascertain internal localization of endogenous SIMPLE (Figure 2F). We found that endogenous SIMPLE located within exosomes was more resistant to limited trypsin digest as compared with other surface-bound exosome proteins, such as Hsp70 and Hsc70 (Figure 2F). Indeed, SIMPLE present inside intact exosomes was more resistant to trypsin digestion than solubilized SIMPLE present in cell lysate (Figure 2G). These data support the notion that SIMPLE is localized inside the exosomes.

Next we examined the role of signature binding motifs proposed for endocytic trafficking (Figure 1A) in secretion of SIMPLE via exosomes (Figure 3). Ala replacement of the di-Leu (LL) [$LL^{154,155}AA$] and YKRL [$YL^{158,161}AA$] motifs abolished secretion of SIMPLE (Figure 3A). Similarly, Ala replacement of the PTAP motif [$PP^{17,20}AA$], to abolish binding of ESCRT1 protein Tsg101, also reduced secretion of SIMPLE (Figure 3B). SIMPLE also encodes two PPxY motifs for recruitment of Nedd4 type E3 ubiquitin ligases, such as Nedd4 and ITCH (Shirk *et al.*, 2005; Eaton *et al.*, 2011). Unexpectedly, Ala replacement of the PPxY motifs [$YY^{23,61}AA$] potentiated the secretion of SIMPLE (Figure 3B). These data indicate that signature motifs known for endocytic trafficking functions are required to achieve proper secretion of SIMPLE via exosomes.

The presence of positive and negative regulatory motifs suggests a differential regulation in SIMPLE secretion. We tested this hypothesis by combined Ala replacement of PPxY and PTAP motifs on SIMPLE [$YY^{23,61}AA$ + $PP^{17,20}AA$] and examined its secretion via exosomes. Ablation of both Nedd4- and Tsg101-binding motifs [$YY^{23,61}AA$ + $PP^{17,20}AA$] did not rescue the impaired secretion of Tsg101 binding–defective [$PP^{17,20}AA$] SIMPLE (Figure 3C). Similarly, combined Ala replacement of PPxY and LL motifs [$YY^{23,61}AA$ + $LL^{154,155}AA$] or PPxY and YKRL motifs [$YY^{23,61}AA$ + $YL^{158,161}AA$] on SIMPLE did not rescue the impaired secretion of [$LL^{154,155}AA$] SIMPLE or [$YL^{158,161}AA$] SIMPLE (data not shown). These data indicate that regulation of SIMPLE secretion by proteins that bind to these endocytic motifs (PTAP, LL, and YKRL) dominates over the role of the PPxY motifs, which facilitate the recruitment of Nedd4 type E3 ubiquitin ligases.

Quantification of exosome secretion using the C2 phosphatidylserine-binding domain of lactadherin

The presence of signature motifs required for endocytic trafficking (Figure 3) and the unique intraluminal position in MVBs and inside exosomes (Figures 1 and 2) suggested that SIMPLE might play a role in the formation of these nanovesicles. To determine whether SIMPLE modulates exosome production in transiently transfected

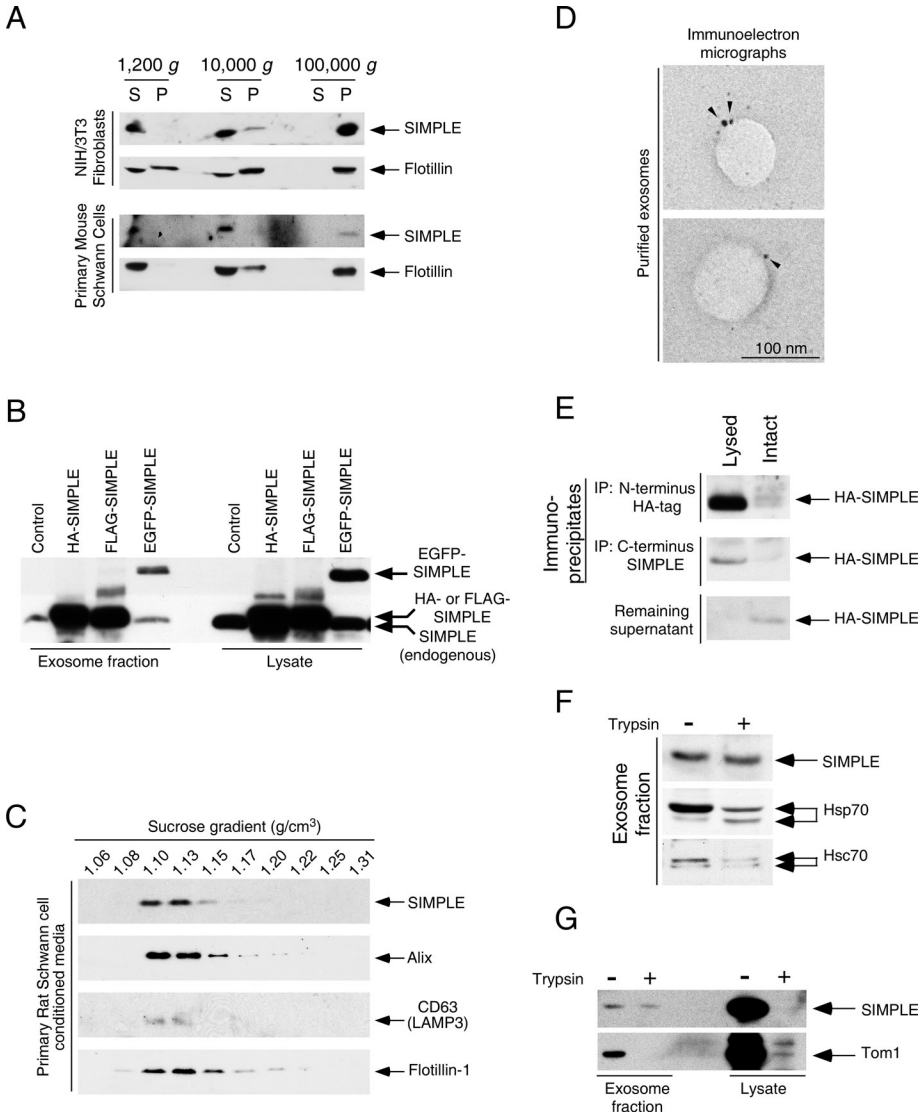

FIGURE 2: Localization of SIMPLE inside exosomes. (A) Conditioned media from NIH 3T3 fibroblasts and primary mouse Schwann cells were subjected to differential centrifugation to isolate exosome pellets. The presence of endogenous SIMPLE and flotillin was detected by immunoblotting. Five percent of supernatant (S) and 10% of SDS-solubilized pellets (P) were examined after each step of centrifugation. (B) COS cells were transiently transfected with different versions of epitope-tagged SIMPLE. Conditioned media from transfected cells were subjected to differential centrifugation to isolate exosome pellets. The presence of endogenous and exogenous SIMPLE in exosome fractions and in cell lysates was detected by immunoblotting. Forty percent of exosome fraction and 4% of cell lysate were examined. (C) Exosome pellets purified from conditioned media of rat primary Schwann cells were subjected to sucrose density gradient ultracentrifugation. Ten fractions were collected and the presence of endogenous SIMPLE, Alix, CD63, and flotillin were determined by immunoblotting. (D) Immuno–electron microscopy was performed to determine the localization of SIMPLE (arrowheads) in purified exosomes isolated from transfected COS cells. Scale bar, 100 nm. (E) Exosome pellets purified from conditioned media of HA-SIMPLE–transfected COS cells were subjected to immunoprecipitations. The presence of HA-SIMPLE in precipitates and remaining supernatant was determined by immunoblotting using antibody against the HA epitope. (F) Exosome pellets purified from conditioned media of COS cells were subjected to limited trypsin digestion. The presence of remaining endogenous SIMPLE, Hsp70, and Hsc70 was determined by immunoblotting. (G) Exosome pellets purified from conditioned media of COS cells or solubilized cell lysate were subjected to trypsin digestion. Levels of SIMPLE and ESCRT-0 protein Tom1 was determined by immunoblotting.

cells, we used the C2 phosphatidylserine-binding domain isolated from lactadherin (LactC2; Yeung *et al.*, 2008) in a fluorescence reporter assay (LactC2–red fluorescent protein [RFP] or LactC2-GFP) to quantify the amount of secreted exosomes (Supplemental Figure S1 and Figure 4). The rationale of using LactC2-fluorescence reporter in quantifying exosome release in transiently transfected cells is in parallel to the common use of promoter-luciferase reporter cassette in gene transcription assays.

Sucrose gradient floatation assays indicated that fluorescence signal derived from the LactC2-RFP was enriched in density where exosomes were localized, whereas only background fluorescence signal was detected in other fractions (Supplemental Figure S1A). These data indicate that LactC2-RFP is present in expected exosome fractions. In addition, fluorescence signal derived from the LactC2-RFP reporter was increased in media with higher amounts of transfected DNA plasmids (Supplemental Figure S1B), indicating dose dependence of the fluorescence reporter. More important, administration of the calcium ionophore ionomycin, which facilitates exosome release (Kramer-Albers *et al.*, 2007), increased LactC2-RFP fluorescence signal in conditioned media, confirming the robustness of this transient assay (Supplemental Figure S1C). Hence the fluorescence intensity of LactC2-RFP in conditioned media is responsive to stimuli that elicit exosome release.

We also examined whether LactC2-RFP affects secretion of known exosome proteins. Expression of LactC2-GFP in cells did not affect secretion of Alix while modestly reducing the level of flotillin in exosome fractions (Supplemental Figure S1D). The latter findings might be due to a squelching effect, which is known in using the promoter-luciferase reporter cassette in transient transcription assays (Natesan *et al.*, 1997). Thus recruitment of endogenous flotillin to the limiting membrane of exosomes might be competed by the overexpressed, exosome-targeted LactC2-GFP reporter proteins. Indeed, LactC2-GFP was enriched in exosomes as compared with EGFP (Supplemental Figure S1D). Taken together, these data indicate that LactC2-RFP is a practical fluorescence reporter to quantify exosome production in transient transfection assays.

Increased formation of exosomes by SIMPLE

On cotransfection with varying amounts of exogenous SIMPLE in COS cells, we found increased LactC2-RFP fluorescence signal in conditioned media in a dose-dependent manner (Figure 4A). Of note, administration of ionomycin provided a synergy effect and further augmented LactC2-RFP fluorescence signal in conditioned media harvested from cells expressing exogenous SIMPLE (Figure 4A). Expression of

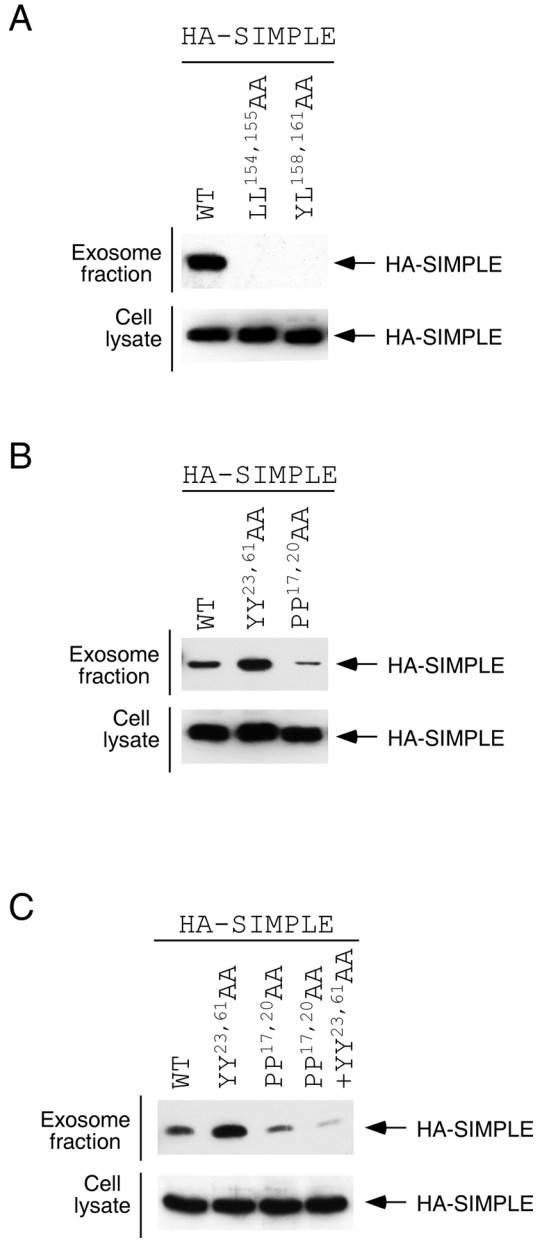

FIGURE 3: Exosome trafficking of SIMPLE. (A) COS cells were transiently transfected with wild-type or [$LL^{154,155}AA$] or [$YL^{158,161}AA$] mutated SIMPLE to investigate the role of LL and YKRL motifs in exosome targeting of SIMPLE. The presence of HA-SIMPLE in exosomes and in cell lysate was determined by immunoblotting using antibody against the HA epitope. Forty percent of exosome fraction and 4% of cell lysate were examined. (B) COS cells were transiently transfected with wild-type or [$YY^{23,61}AA$] or [$PP^{17,20}AA$] mutated SIMPLE to determine the role of Nedd4 type E3 ubiquitin ligases and Tsg101 in exosome targeting of SIMPLE. The presence of HA-SIMPLE in exosomes and in cell lysate was determined by immunoblotting using antibody against the HA epitope. Forty percent of exosome fraction and 4% of cell lysate were examined. (C) COS cells were transiently transfected with wild-type, Nedd4 binding–defective [$YY^{23,61}AA$], Tsg101 binding–defective [$PP^{17,20}AA$] or combination of Nedd4 binding–defective and Tsg101 binding–defective [$YY^{23,61}AA$ + $PP^{17,20}AA$] SIMPLE. The presence of HA-SIMPLE in exosomes and in cell lysate was determined by immunoblotting using antibody against the HA epitope. Forty percent of exosome fraction and 4% of cell lysate were examined.

different tagged versions of exogenous SIMPLE, as well as the *Caenorhabditis elegans* orthologue, also increased LactC2-RFP fluorescence reporter in conditioned media (Figure 4B). We also confirmed increased secretion of LactC2 domain after the expression of exogenous SIMPLE, using immunoblotting to detect LactC2-GFP in exosomes (Figure 4C). To quantify the amount of secreted exosomes in the presence and absence of exogenous SIMPLE, we further performed nanoparticle tracking analysis (Figure 4D). Conditioned media harvested from cells expressing exogenous SIMPLE showed increased concentration of exosomes as compared with mock-transfected cells (Figure 4D). In addition, CD63 and Alix, proteins previously found in exosomes, were enriched in exosomes isolated from cells expressing exogenous SIMPLE (Figure 4E). The level of flotillin in exosomes, however, seems unaffected (Figure 4E). Taken together, these data indicate that expression of SIMPLE increases the number of exosomes and secretion of specific exosome proteins.

Genetic models of SIMPLE

We sought to determine whether this newly established role for SIMPLE in exosome production might feature in the onset or progression of CMT1C. Thus we examined the effect of different CMT1C genotypes on exosome formation (Street *et al.*, 2003; Saifi *et al.*, 2005; Latour *et al.*, 2006; Gerding *et al.*, 2009). We introduced by gene targeting a single point mutation in floxed exon 3 of the *Simple* gene to convert the codon Thr115 (ACC) to that for Asn (AaC; T115N) and model CMT1C disease (Figure 5, A and B). This knock-in approach was specifically selected to exclude the complications encountered with an overexpression model, particularly as the basis of dominant inheritance in CMT1C is unknown. Removal of floxed exon 3 was carried out by Cre-mediated recombination to generate SIMPLE-null mice ($Simple^{-/-}$). PCR analysis indicated successful creation of $Simple^{T115N/+}$, $Simple^{T115N/T115N}$, and $Simple^{+/-}$ genotypes (Figure 5, C–E). Immunoblotting analysis revealed similar levels of SIMPLE protein in primary mouse embryonic fibroblasts (MEFs) with $Simple^{+/+}$, $Simple^{T115N/+}$, and $Simple^{T115N/T115N}$ genotypes (Figure 5F). In $Simple^{-/-}$ MEFs, expression of SIMPLE protein was not detected (Figure 5F).

With a physiological model that expresses mutated SIMPLE at endogenous levels, we asked whether the localization of SIMPLE in late endosomes/MVBs/lysosomes was affected upon CMT1C mutation (Figure 6). We found similar punctated staining with partial colocalization of endogenous SIMPLE and LAMP1 in $Simple^{+/+}$, $Simple^{T115N/+}$, and $Simple^{T115N/T115N}$ MEFs (Figure 6, A and B). Punctated staining of SIMPLE was not detected in $Simple^{-/-}$ MEFs (Figure 6A), confirming the effective of ablation in $Simple^{-/-}$ (Figure 5F). We further separated cytosolic and membrane fractions to ascertain the localization of endogenous SIMPLE upon CMT1C mutation (Figure 6C). As expected, endogenous SIMPLE expressed in $Simple^{+/+}$ and $Simple^{T115N/+}$ MEFs was detected in membrane fraction along with known membrane-associated protein LAMP1 (Figure 6C). Soluble proteins, such as Hsp70 and tubulin, were found exclusively in cytosolic fractions where no SIMPLE was detected (Figure 6C). Small GTPases Rab5 and Rab7 were detected in both membrane and cytosolic fractions, as reported previously (Figure 6C; Felberbaum-Corti *et al.*, 2005; Wang *et al.*, 2011). Taken together, these data indicate that neither the expression level of SIMPLE (Figure 5F) nor its subcellular distribution (Figure 6) is affected by CMT1C mutation.

CMT1C mutation impairs exosome localization of SIMPLE

Despite similar levels of endogenous SIMPLE in the cell lysates, we found that the amount of secreted SIMPLE present in exosomes

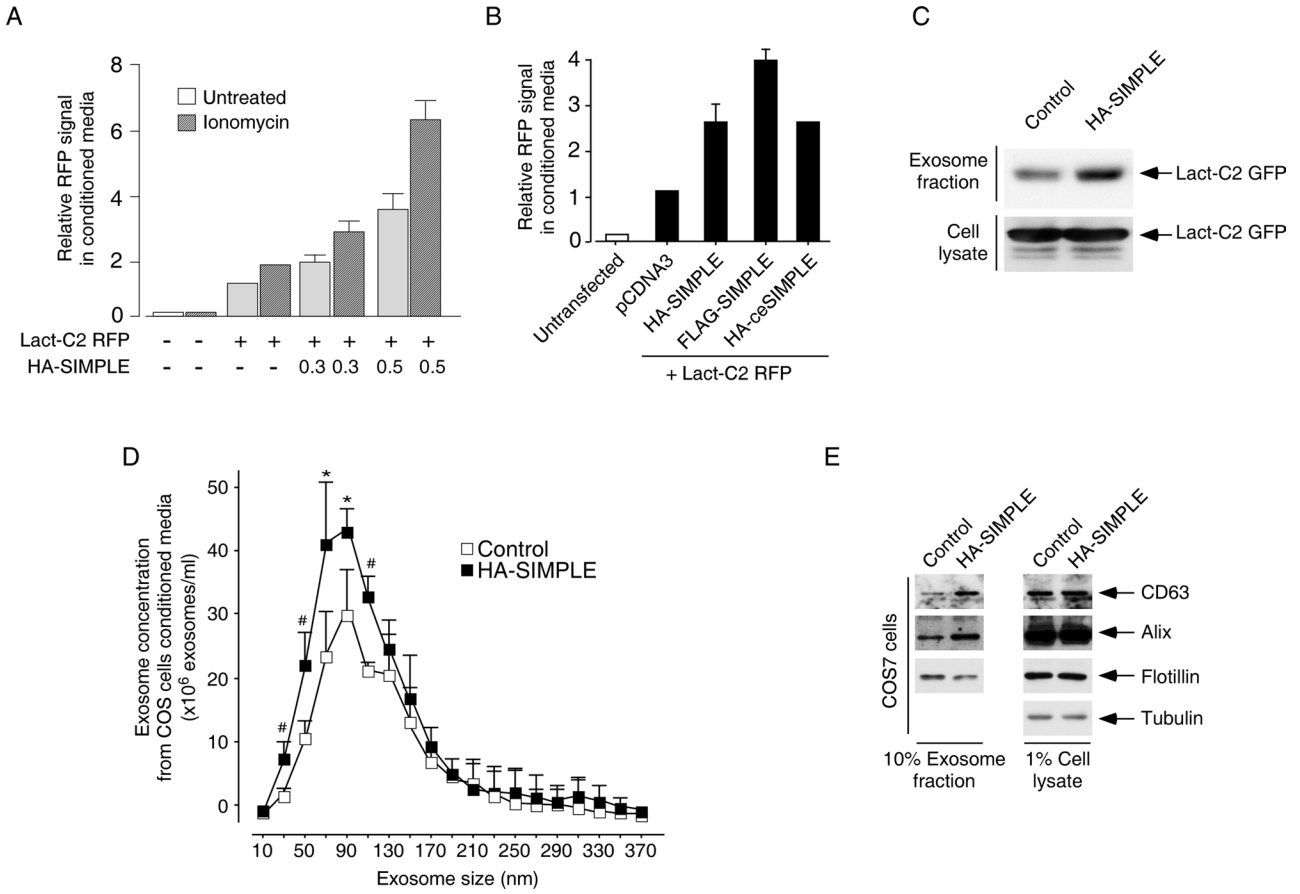

FIGURE 4: Increased formation of exosomes by SIMPLE. (A) COS cells were transiently transfected with HA-SIMPLE and LactC2-RFP reporter. Cells were stimulated or not with ionomycin, and relative RFP signals in conditioned media were determined on microplate reader (mean ± SD; $n = 3$). (B) LactC2-RFP reporter was transiently cotransfected with different versions of epitope-tagged SIMPLE into COS cells. Relative levels of RFP in conditioned media of transfected cells were determined on microplate reader (mean ± SD; $n = 3$). (C) COS cells were transiently transfected with HA-SIMPLE and LactC2-GFP reporter. The levels of GFP in isolated exosomes were determined by immunoblotting. (D) COS cells were mock transfected (Control) or transiently transfected with HA-SIMPLE. Nanoparticle tracking analysis was performed to quantify the amount of secreted exosomes present in conditioned media. $^{*}p < 0.05$; $^{\#}p < 0.005$. (E) COS cells were transiently transfected with HA-SIMPLE and vector control. The levels of CD63, Alix, and flotillin in isolated exosomes were determined by immunoblotting. Expression levels of tubulin were used as controls. Ten percent of exosome fraction and 1% of cell lysate were examined.

was reduced for *Simple*$^{T115N/+}$ and *Simple*$^{T115N/T115N}$ MEFs versus *Simple*$^{+/+}$ MEFs (Figure 7A). Relative to the exogenous wild-type SIMPLE, similar reduction of secreted SIMPLE in exosomes was found in cells exogenously expressing other CMT1C isoforms [A^{111}G, G^{112}S, T^{115}N, W^{116}G, P^{135}S, P^{135}T and V^{144}M] (Figure 7, B and C). Substitutions in SIMPLE, T^{49}M and L^{122}V, however, did not affect secretion of SIMPLE (Figure 7B), suggesting that these changes might represent rare polymorphisms. More important, secretion of exogenously expressed, CMT1C-mutated SIMPLE was also greatly impaired as compared with its wild-type counterpart in rat primary Schwann cells (Figure 7D). These data indicate that SIMPLE mutations strongly associated with CMT1C abrogate exosomal localization of SIMPLE.

We also tested whether removal of Nedd4-binding motif [YY^{23,61}AA], which increased the presence of SIMPLE in exosomes (Figure 3), modulates secretion of CMT1C-mutated SIMPLE. Thus we generated combined Ala replacement of PPxY and CMT1C mutation on SIMPLE ([YY^{23,61}AA + A^{111}G], [YY^{23,61}AA + G^{112}S], [YY^{23,61}AA + T^{115}N], and [YY^{23,61}AA + P^{135}S]). Unexpectedly, removal of Nedd4 binding partially rescued and improved exosomal secretion of CMT1C-mutated SIMPLE (Figure 7E). These data indicate that the role of Nedd4 type E3 ligases dominates over CMT1C mutation in regulating exosome secretion of SIMPLE. Perhaps modulating Nedd4 type E3 ubiquitin ligases is beneficial for CMT1C.

Changes in the secretion of exosomes upon CMT1C mutation

Next we performed scanning electron microscopy to visualize secreted exosomes from *Simple*$^{+/+}$ and *Simple*$^{T115N/+}$ MEFs (Figure 8A). We found that exosomes were readily detected in *Simple*$^{+/+}$ MEFs. As expected, the size of exosomes isolated from *Simple*$^{+/+}$ MEFs were ~100 nm in diameter (Figure 8A). Exosomes isolated from *Simple*$^{T115N/+}$ MEFs, however, were smaller, and many of them were <40 nm in diameter (Figure 8A). In addition to the smaller size, there were fewer exosomes in *Simple*$^{T115N/+}$ MEFs (Figure 8A). To quantify secreted exosomes from *Simple*$^{+/+}$ and *Simple*$^{T115N/+}$ MEFs, we carried out morphometric determination to count the number and determine the size of exosomes in multiple electron micrographs (Figure 8B). We also performed nanoparticle tracking analysis to

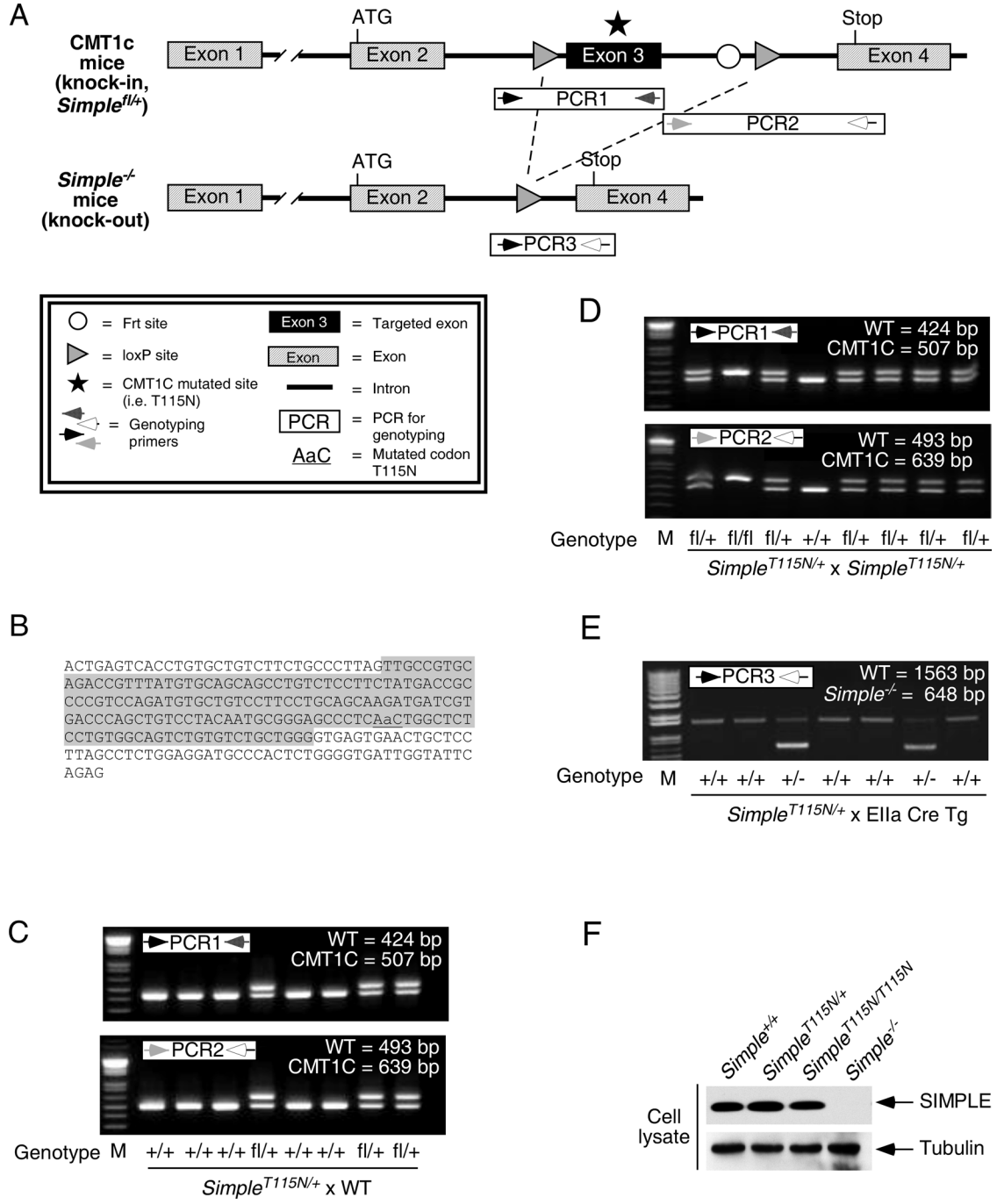

FIGURE 5: Genetic models of SIMPLE. (A) Schematic illustration of the knock-in SIMPLE locus harboring CMT1C mutation (fl/+, *Simple*$^{T115N/+}$). Cre-mediated deletion of exon 3 to generate *Simple*$^{-/-}$ phenotype is also shown. (B) A C>A point mutation (underlined) was introduced into codon 115 in exon 3 (highlighted) of the *Simple* gene to mutate the amino acid from Thr to Asn (T115N). (C) PCR genotyping for the generation of *Simple*$^{T115N/+}$ (fl/+) mice. (D) PCR genotyping for the generation of *Simple*$^{T115N/+}$ (fl/+) and *Simple*$^{T115N/T115N}$ (fl/fl) mice. (E) PCR genotyping for the generation of *Simple*$^{+/-}$ mice. (F) Expression levels of endogenous SIMPLE in *Simple*$^{+/+}$, *Simple*$^{T115N/+}$, *Simple*$^{T115N/T115N}$, and *Simple*$^{-/-}$ MEFs were analyzed by immunoblotting. Expression levels of tubulin were used as controls.

ascertain the changes in overall exosome profile of *Simple*$^{+/+}$ and *Simple*$^{T115N/+}$ MEFs (Figure 8C). Morphometric determination ascertained that the bulk of exosomes secreted from *Simple*$^{T115N/+}$ MEFs were smaller (Figure 8B). In addition, morphometric determination and nanoparticle tracking analysis confirmed that fewer exosomes were secreted from *Simple*$^{T115N/+}$ MEFs (Figure 8, B and C). Decreased exosome concentration was also found in mouse plasma prepared from *Simple*$^{T115N/+}$ mice as compared with *Simple*$^{+/+}$ mouse plasma (Figure 8D). These data indicate that secretion of exosomes is compromised upon CMT1C mutation of endogenous SIMPLE. These data also support a role of SIMPLE in regulating exosome production (Figure 4).

We also examined the level of exosome proteins secreted by *Simple*$^{+/+}$ and *Simple*$^{T115N/+}$ MEFs. We found that the level

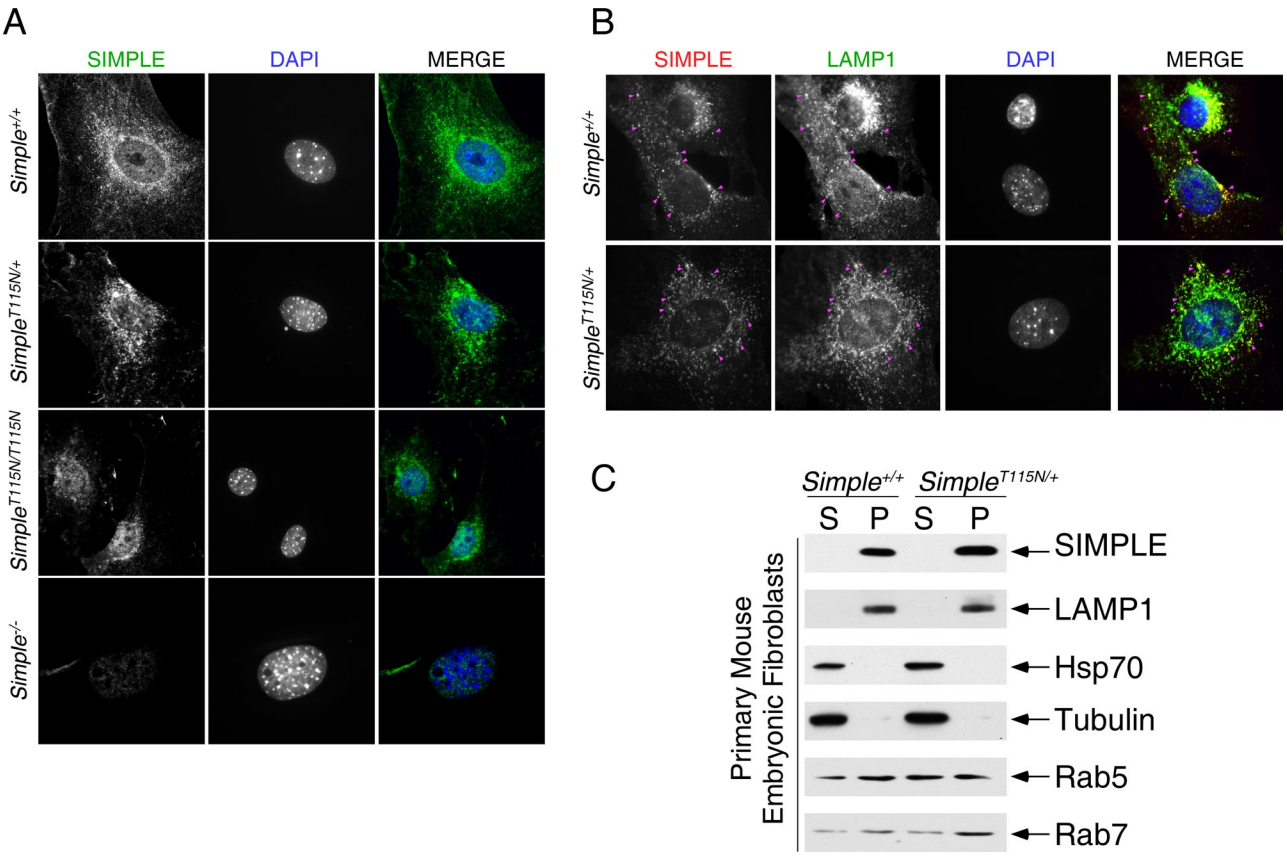

FIGURE 6: Localization of endogenous CMT1C-mutated SIMPLE. (A) Staining of endogenous SIMPLE (green) in *Simple*$^{+/+}$, *Simple*$^{T115N/+}$, *Simple*$^{T115N/T115N}$, and *Simple*$^{-/-}$ MEFs was analyzed by immunofluorescence microscopy. DNA in nuclei was visualized using DAPI (blue). (B) Costaining of endogenous SIMPLE (red) and LAMP1 (green) in *Simple*$^{+/+}$ and *Simple*$^{T115N/+}$ MEFs was analyzed by immunofluorescence microscopy. DNA in nuclei was visualized using DAPI (blue). Arrows point to colocalization of SIMPLE and LAMP1. (C) *Simple*$^{+/+}$ and *Simple*$^{T115N/+}$ MEFs were extracted with hypotonic buffer to prepare cytosolic extract (S). Membrane fraction (P) was also collected after centrifugation at 100,000 × *g*. Localization of SIMPLE, LAMP1, Hsp70, tubulin, Rab5, and Rab7 in cytosol (S) and in membrane fraction (P) was determined by immunoblotting.

of known exosome proteins, including Alix, flotillin, and Hsp70, in *Simple*$^{T115N/+}$ exosomes was reduced (Figure 8E). The level of clathrin heavy chain in exosomes, however, was similar for both genotypes (Figure 8E). These data indicate that SIMPLE regulates exosome production and also suggest that mutation of SIMPLE likely affects a subset of exosomes.

Defects in endosomal/lysosomal compartments upon CMT1C mutation

Exosomes are derived, in part, from the extracellular release of intraluminal vesicles upon fusion of MVBs with plasma membrane (Simons and Raposo, 2009; Huotari and Helenius, 2011). Given that SIMPLE resides inside intraluminal vesicles of MVBs, changes in the landscape of exosome profile upon CMT1C mutation might affect the formation of MVBs. Indeed, electron microscopy showed that typical multivesicular appearances of MVBs were rarely identified in *Simple*$^{T115N/+}$ MEFs (Figure 9A). Instead, in *Simple*$^{T115N/+}$ MEFs, we found either the presence of empty vacuoles without obvious intraluminal vesicles or enlarged vacuoles containing electron-dense granules inside (Figure 9A). Multilamellar cisternal compartments near the vacuoles, hallmarks of *vps* mutants with defective MVBs (Raymond *et al.*, 1992; Rieder *et al.*, 1996), were also found in *Simple*$^{T115N/+}$ MEFs (Figure 9A). In *Simple*$^{+/+}$ MEFs, as expected, compartments containing intraluminal vesicles, indicative of MVBs, were evident (Figure 9A). These data indicate that CMT1C mutation of SIMPLE generates a vacuolated appearance in MVBs.

We also examined the cellular ultrastructure in *Simple*$^{-/-}$ and *Simple*$^{T115N/T115N}$ MEFs (Figure 9A). Similar to *Simple*$^{T115N/+}$ MEFs, typical multivesicular appearances of MVBs were rarely identified in *Simple*$^{-/-}$ and *Simple*$^{T115N/T115N}$ MEFs (Figure 9, A and B). Indeed, reduced exosome secretion and decreased levels of exosome proteins were found in *Simple*$^{-/-}$ and *Simple*$^{T115N/T115N}$ MEFs (Supplemental Figure S2). In *Simple*$^{-/-}$ MEFs, however, vacuolated appearance was not as evident as in *Simple*$^{T115N/+}$ MEFs (Figure 9, A and B). Instead, the presence of multilamellar cisternal compartments and accumulation of electron-dense granules in *Simple*$^{-/-}$ MEFs were more apparent than with *Simple*$^{T115N/+}$ MEFs (Figure 9, A and B).

In *Simple*$^{T115N/T115N}$ MEFs, vacuolated appearances in MVBs were manifested as in *Simple*$^{T115N/+}$ MEFs (Figure 9, A and B). The presence of multilamellar cisternal compartments and accumulation of electron-dense granules in *Simple*$^{T115N/T115N}$ MEFs, however, were more evident than in *Simple*$^{T115N/+}$ MEFs (Figure 9, A and B). Indeed, the appearances of multilamellar cisternal compartments and accumulation of electron-dense granules in *Simple*$^{T115N/T115N}$ MEFs were comparable to those in *Simple*$^{-/-}$ MEFs (Figure 9B).

Taken together, these data demonstrate a role of SIMPLE in MVBs. In particular, all three genetic models (*Simple*$^{T115N/+}$,

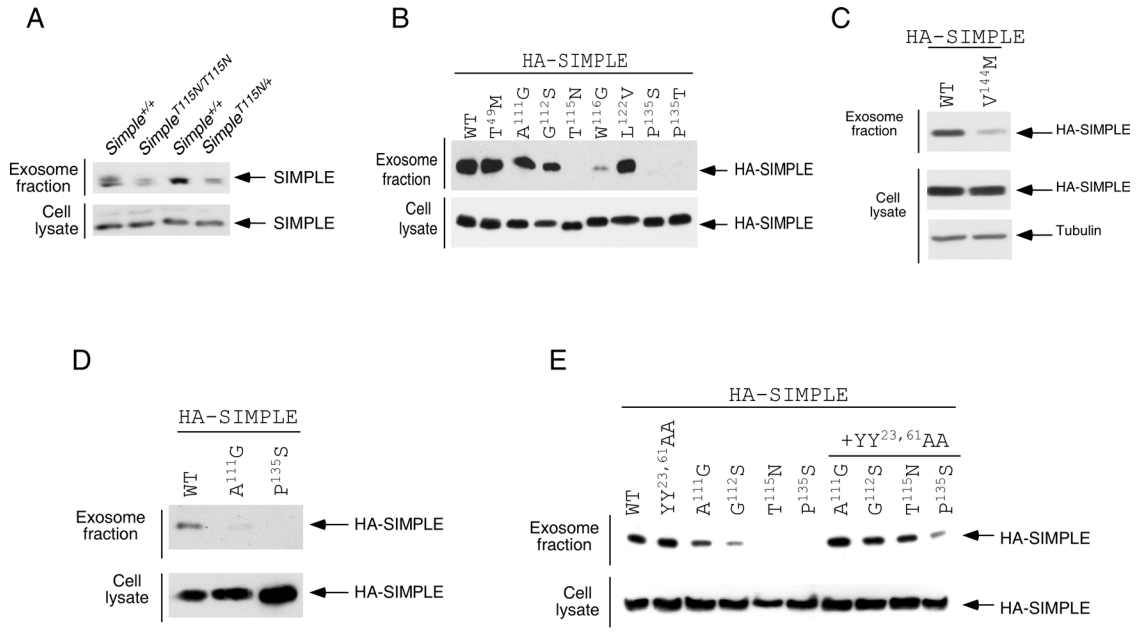

FIGURE 7: Effects of CMT1C mutation on secretion of SIMPLE via exosomes. (A) The levels of endogenous SIMPLE in secreted exosomes and in cell lysates of *Simple*$^{+/+}$, *Simple*$^{T115N/+}$, and *Simple*$^{T115N/T115N}$ MEFs were determined by immunoblotting. (B) COS cells were transiently transfected with wild-type (WT) or mutated SIMPLE. The presence of HA-SIMPLE in exosomes and in cell lysate was determined by immunoblotting using antibody against the HA epitope. Known CMT1C mutations include A^{111}G, G^{112}S, T^{115}N, W^{116}G, P^{135}S, and P^{135}T. Both T^{49}M and L^{122}V likely represent a low frequency of polymorphisms in SIMPLE. Forty percent of exosome fraction and 4% of cell lysate were examined. (C) COS cells were transiently transfected with WT or V^{144}M CMT1C-mutated SIMPLE. The presence of HA-SIMPLE in exosomes and in cell lysate was determined by immunoblotting using antibody against the HA epitope. Forty percent of exosome fraction and 4% of cell lysate were examined. (D) Rat primary Schwann cells were infected with WT or CMT1C-mutated (A^{111}G and P^{135}S) SIMPLE. The presence of HA-SIMPLE in exosomes and in cell lysate was determined by immunoblotting using antibody against the HA epitope. Forty percent of exosome fraction and 4% of cell lysate were examined. (E) COS cells were transiently transfected with wild-type SIMPLE or SIMPLE carrying Ala replacement at the Nedd4-binding motif [YY^{23,61}AA], SIMPLE with CMT1C mutation [A^{111}G, G^{112}S, T^{115}N, or P^{135}S], or SIMPLE with combination of Nedd4-binding defect and CMT1C mutation [YY^{23,61}AA + CMT1C mutation] ([YY^{23,61}AA + A^{111}G], [YY^{23,61}AA + G^{112}S], [YY^{23,61}AA + T^{115}N], and [YY^{23,61}AA + P^{135}S]). The presence of HA-SIMPLE in exosomes and in cell lysate was determined by immunoblotting using antibody against the HA epitope. Forty percent of exosome fraction and 4% of cell lysate were examined.

Simple$^{-/-}$, and *Simple*$^{T115N/T115N}$ MEFs) show defects in exosome production (Figure 8 and Supplemental Figure S2). Furthermore, these data indicate that CMT1C mutation of SIMPLE (*Simple*$^{T115N/+}$ and *Simple*$^{T115N/T115N}$) leads to different ultrastructural changes as compared with the loss of expression of SIMPLE (*Simple*$^{-/-}$), suggesting the possibility that CMT1C-associated mutation may impart a partial toxic gain of function.

We also performed immunofluorescence analysis to examine the appearances of other endosomal compartments in *Simple*$^{+/+}$ and *Simple*$^{T115N/+}$ MEFs. Confocal microscopy indicated that LAMP1-stained (Figure 5H) or LAMP2-stained (Figure 10, A and B) lysosomal compartments were more apparent and appeared enlarged in *Simple*$^{T115N/+}$ MEFs as compared with *Simple*$^{+/+}$ MEFs. Confocal microscopy also indicated more apparent staining of Rab7 in late endosomes in *Simple*$^{T115N/+}$ MEFs (Figure 10C). Rab7-stained, late endosomal compartments also appeared enlarged in *Simple*$^{T115N/+}$ MEFs (Figure 10C). LBPA-stained MVB compartments, however, seemed indistinguishable between *Simple*$^{+/+}$ and *Simple*$^{T115N/+}$ MEFs (Figure 10, C and D). Early endosomes, as indicated by staining of EEA1, appeared diffused, with smaller punctae in *Simple*$^{T115N/+}$ MEFs (Figure 10, B and D). Costaining of EEA1 with either LBPA or LAMP2 confirmed distinct compartmentalization of early endosomes, late endosomes, and lysosomes (Figure 10, B and D). Taken together, electron microscopy (Figure 9) and immunofluorescence assays (Figure 10) indicate that CMT1C mutation elicits changes in structure and appearance in endosomes, MVBs, and lysosomes without disturbing the expression and localization of SIMPLE (Figures 5 and 6).

Reduced exosomal trafficking and aberrant endosomal/lysosomal compartments in CMT1C patient B cells

Next we examined secretion of SIMPLE in exosomes from CMT1C patient B cells (Shirk *et al.*, 2005) to compare it with results from CMT1C mouse cells. Analogous to the CMT1C MEFs (Figure 5F), endogenous levels of SIMPLE protein were similar in control and CMT1C B cell lysates (Figure 11A). As expected, control B cells showed secretion of SIMPLE via exosomes, which was further increased by ionomycin (Figure 11A). The levels of secreted SIMPLE in exosomes, however, were reduced in CMT1C patient B cells, even in the presence of ionomycin (Figure 11A). Scanning electron microscopy and morphometric determination, to count the number and determine the size of exosomes, further revealed fewer and smaller exosomes in CMT1C patient B cells (Figure 11, B and C). In addition, nanoparticle tracking analysis ascertained that the concentration of exosomes secreted by CMT1C patient B cells was reduced as compared with their control counterparts (Figure 11D). Furthermore, the level of known exosome proteins, such as Alix and CD63,

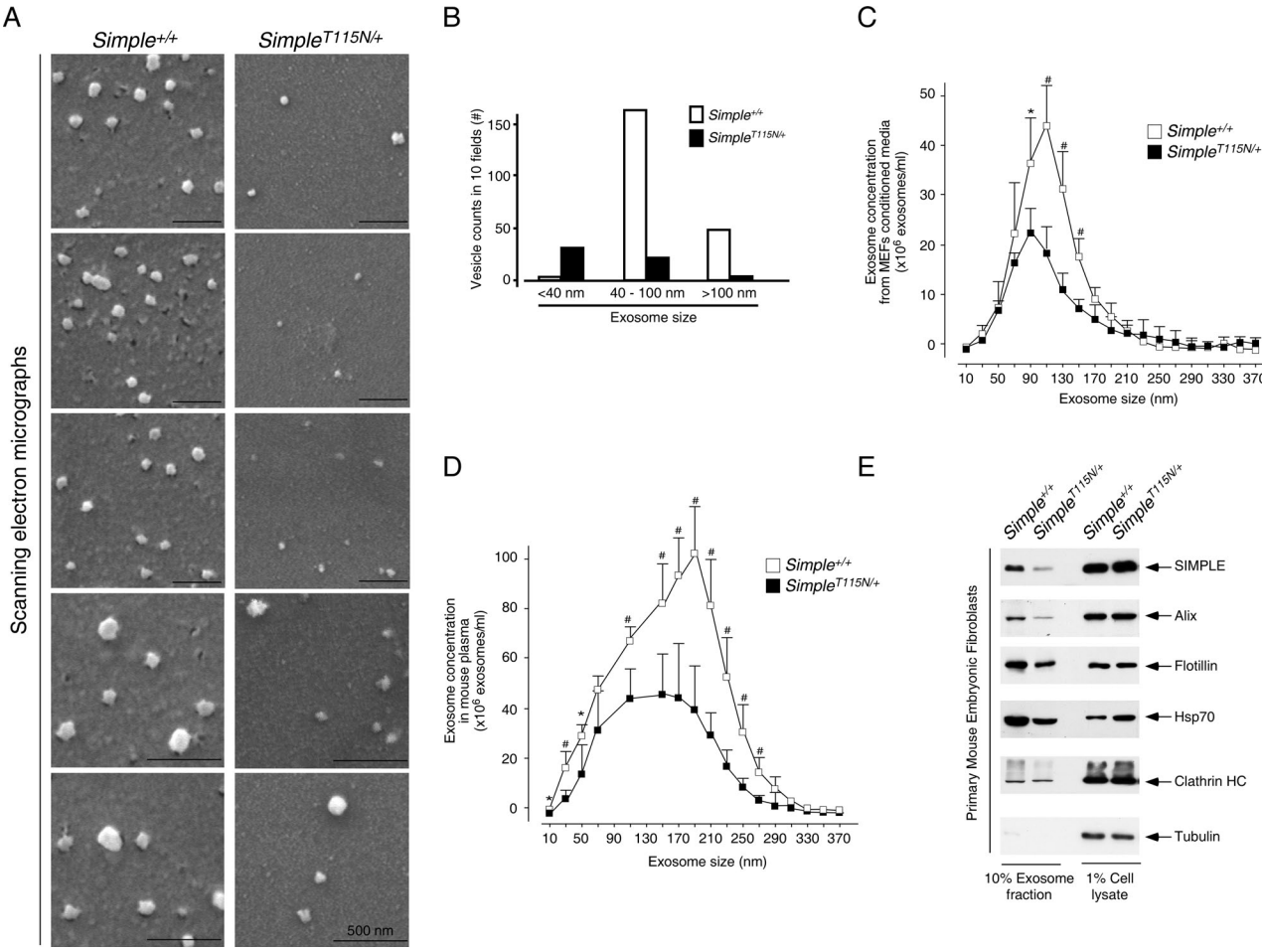

FIGURE 8: Reduced secretion of exosomes upon CMT1C mutation. (A) Scanning electron microscopy was performed to reveal the appearance of exosomes secreted by *Simple*$^{+/+}$ and *Simple*$^{T115N/+}$ MEFs. Representative images are shown. Scale bar, 500 nm. (B) Morphometric determination was performed to count the number and determine the size of exosomes from 10 photos taken from different fields of the EM grids. (C) Exosomes present in conditioned media of *Simple*$^{+/+}$ and *Simple*$^{T115N/+}$ MEFs were quantified by nanoparticle tracking analysis. (D) Exosomes from plasma of *Simple*$^{+/+}$ and *Simple*$^{T115N/+}$ mice were prepared and quantified by nanoparticle tracking analysis. $^{*}p < 0.05$; $^{\#}p < 0.005$. (E) Exosome proteins secreted from *Simple*$^{+/+}$ and *Simple*$^{T115N/+}$ MEFs were determined by immunoblotting. Ten percent of exosome fractions and 1% of cell lysate were examined.

was reduced in the exosomes of CMT1C patient B cells (Figure 11E). Similar to *Simple*$^{+/+}$ and *Simple*$^{T115N/+}$ MEFs, the level of clathrin heavy chain in exosomes isolated from control and CMT1C patient B cells was similar (Figure 11E). These data confirm that, in both mouse and human cells, CMT1C mutation reduces the localization of endogenous SIMPLE in exosomes without obvious effect on its expression. CMT1C mutation also causes production of smaller exosomes and reduced concentration of secreted exosomes.

CMT1C patient B cells also displayed changes in appearances in endosomal/lysosomal compartments, although localization of endogenous CMT1C-mutated SIMPLE was indistinguishable from wild-type SIMPLE in control cells, as suggested previously (Figure 12A; Shirk *et al.*, 2005). LAMP2-stained lysosomal compartments seemed more intense in CMT1C patient B cells as compared with control B cells (Figure 12A). Staining of Rab7 in late endosomes was manifested in CMT1C patient B cells (Figure 12B), whereas staining of LBPA in MVBs appeared similar (Figure 12, B and C). Indeed, increased Rab7-stained puntae were evident in CMT1C patient B cells (Figure 12D). Staining of EEA1 in early endosomes, however, showed discrete punctae with reduced intensity in CMT1C patient B cells (Figure 12C). Taken together, these data indicate compromised appearances in endosomes, MVBs, and lysosomes of CMT1C patient B cells.

We further ascertained morphological changes in endosomes/MVBs in CMT1C patient B cells by electron microscopy. Representative structures of typical MVBs containing intraluminal vesicles were readily detected in control B cells (Figure 12E). Ultrastructural analysis, however, revealed the presence of enlarged empty vacuoles without obvious intraluminal vesicles in CMT1C patient B cells (Figure 12, E and F). These data confirm that CMT1C mutation elicits defects in production of intraluminal vesicles and generates vacuolated appearances in MVBs.

Defects in endosomal/lysosomal compartments upon CMT1C mutation in primary Schwann cells

CMT1C neuropathy is a peripheral demyelinating disease in patients. Indeed, we observed that some mice harboring CMT1C mutations exhibit paralysis at old age (data not shown; also see *Discussion*). Defects in Schwann cells were suggested to account for the CMT1C neuropathy. To test whether CMT1C mutation also leads to defects in endosomal/lysosomal compartments in Schwann cells,

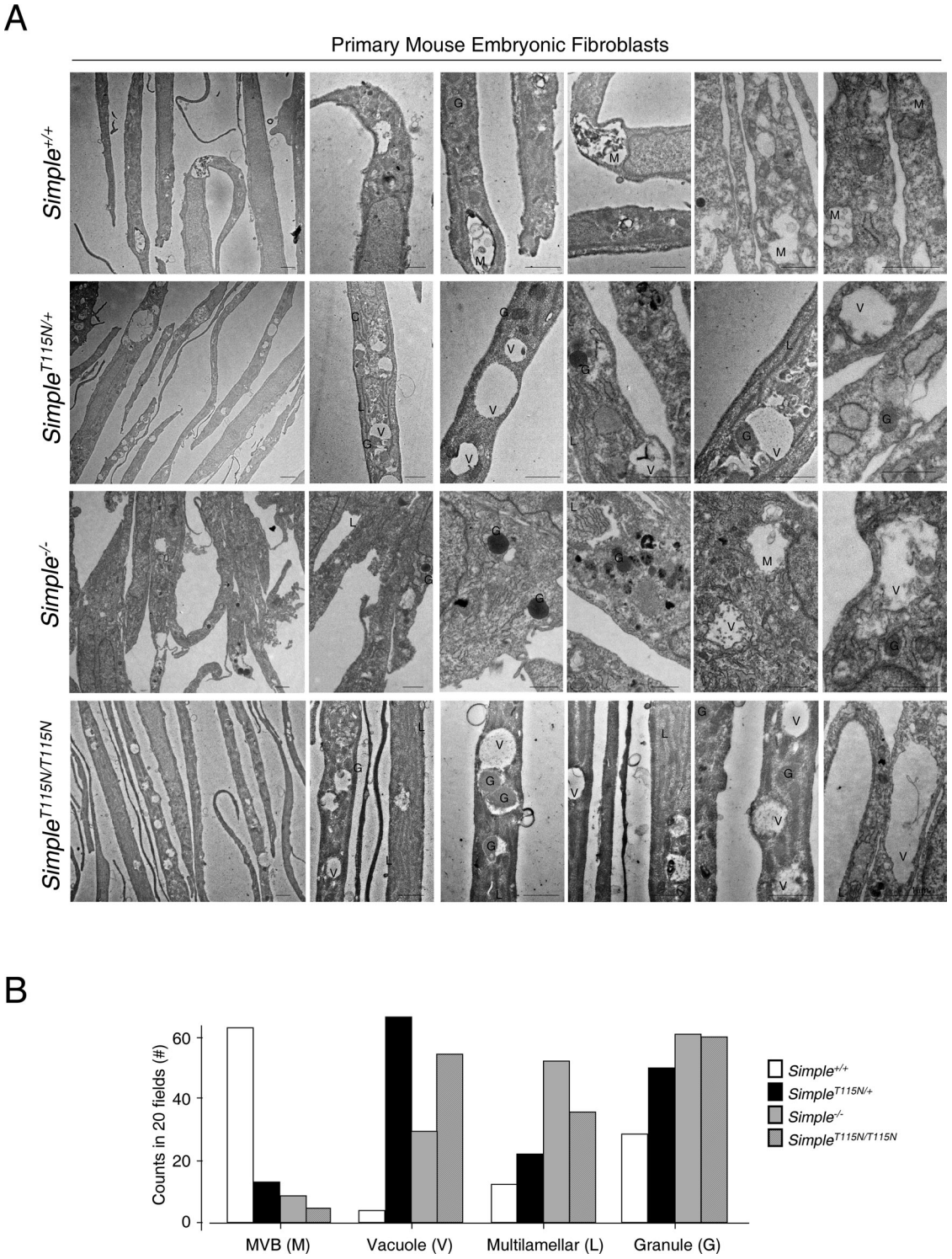

FIGURE 9: Electron microscopy reveals defects in endosomal/lysosomal compartments upon CMT1C mutation. (A) Transmission electron microscopy was performed to determine the ultrastructure of *Simple*$^{+/+}$ and *Simple*$^{T115N/+}$ MEFs. Cellular ultrastructure in *Simple*$^{-/-}$ and *Simple*$^{T115N/T115N}$ MEFs is also shown. Scale bar, 1 μm. (B) Morphometric determination was performed to count the appearances of multivesicular bodies (M), enlarged empty vacuoles (V), multilamellar cisternal compartments (L), and electron-dense granules (G) in 20 photos taken from different fields of the EM grids.

we further used our mice harboring mutation of SIMPLE at the endogenous levels and examined ultrastructures of isolated primary Schwann cells by electron microscopy. Similar to *Simple*$^{T115N/+}$ MEFs and CMT1C patient B cells, electron microscopy analysis revealed the presence of enlarged empty vacuoles without obvious intraluminal vesicles in *Simple*$^{T115N/+}$ Schwann cells (Figure 13A). Electron-dense granules and multilamellar cisternal compartments in *Simple*$^{T115N/+}$ Schwann cells were also evident (Figure 13, A and B).

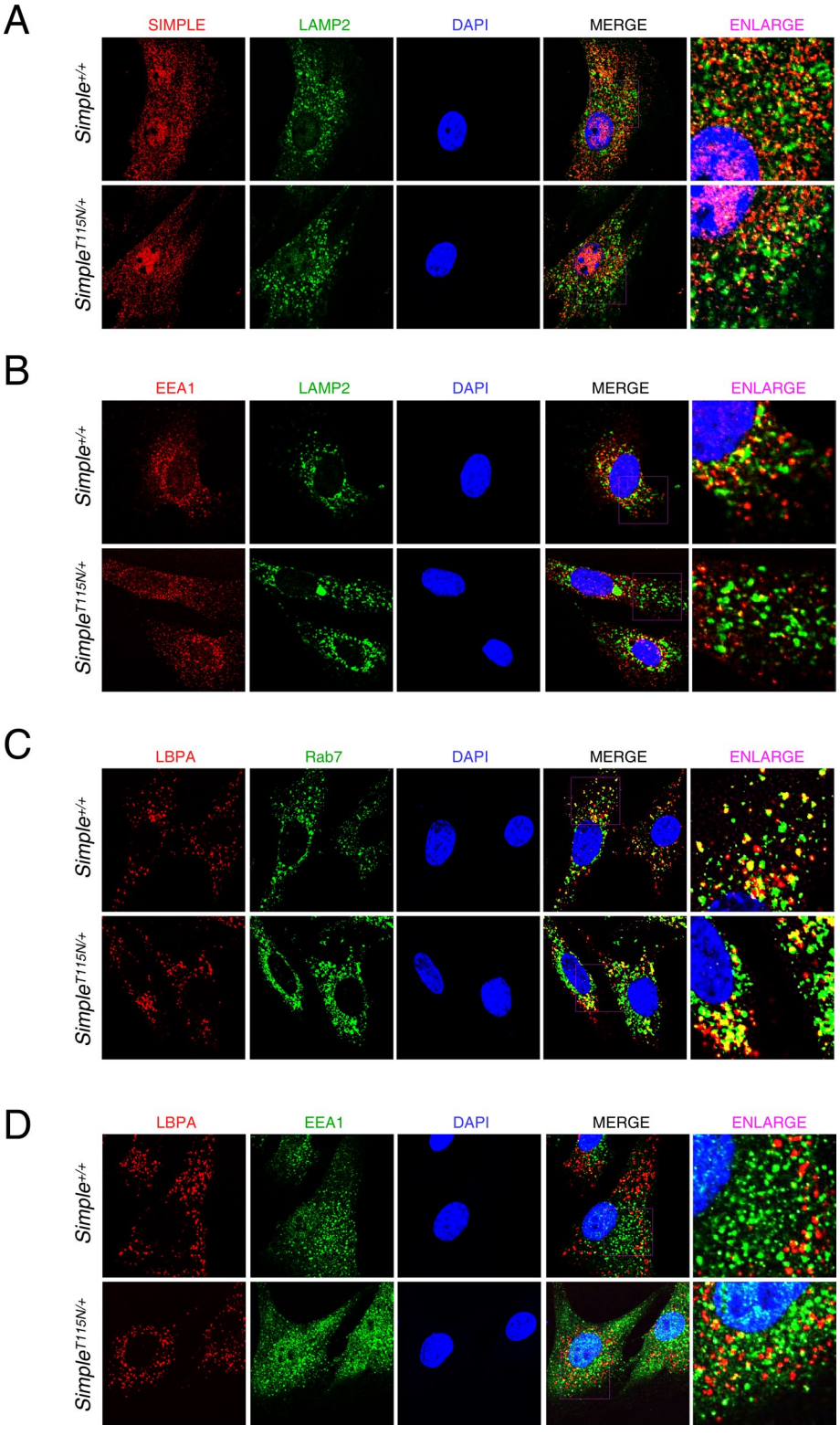

FIGURE 10: Confocal microscopy reveals defects in endosomal/lysosomal compartments upon CMT1C mutation. (A) Costaining of endogenous SIMPLE (red) and LAMP2 (green) in *Simple*$^{+/+}$ and *Simple*$^{T115N/+}$ MEFs was analyzed by confocal microscopy. DNA in nuclei was visualized using DAPI (blue). (B) Costaining of endogenous EEA1 (red) and LAMP2 (green) in *Simple*$^{+/+}$ and *Simple*$^{T115N/+}$ MEFs. (C) Costaining of lysobisphosphatidic acid (LBPA, red) and endogenous Rab7 (green) in *Simple*$^{+/+}$and *Simple*$^{T115N/+}$ MEFs. (D) Costaining of lysobisphosphatidic acid (LBPA, red) and endogenous EEA1 (green) in *Simple*$^{+/+}$and *Simple*$^{T115N/+}$ MEFs.

As expected, typical MVBs containing intraluminal vesicles were readily detected in *Simple*$^{+/+}$, but not in *Simple*$^{T115N/+}$, Schwann cells. Taken together, these data indicate that CMT1C mutation generates vacuolated appearances in MVBs, which contribute to defects in exosome secretion, in multiple cell types.

DISCUSSION

In this article, we show that SIMPLE regulates the production of exosomes. We also show that a single point mutation of endogenous SIMPLE in CMT1C mouse primary cells (MEFs and Schwann cells) and patient B cells alters exosome production. Improper formation of MVBs and accumulation of lysosomes, in part, contribute to the reduced production of exosomes by CMT1C mutation. These findings therefore demonstrate a role of SIMPLE in vesicular trafficking and for the first time a possible mechanistic understanding of CMT1C.

SIMPLE in vesicular trafficking

Our data indicate a role of SIMPLE in exosomes and formation of MVBs. Possible involvement of SIMPLE in microvesicles, however, cannot be excluded. Exosomes and microvesicles are different nanovesicles derived from distinctive cellular compartments. Current models imply that exosomes originate from MVBs, whereas microvesicles derive from shredding of plasma membranes (Huotari and Helenius, 2011; Mittelbrunn and Sanchez-Madrid, 2012). Unfortunately, biochemical characteristics of exosomes and microvesicles are highly similar, in part, due to an integrated circuit for continuous membrane trafficking. Thus it is difficult to identify a specific subset of proteins being secreted by exosomes but not by microvesicles (or vice versa). Given that SIMPLE exhibits punctated intracellular pattern with little staining on the plasma membrane (Figure 6), we surmise that SIMPLE is mainly affecting exosome formation. The presence of signature binding motifs proposed for endocytic trafficking and their positive and negative roles in exosome secretion of SIMPLE also support this model (Figures 3 and 7). Malformation of MVBs in CMT1C mutation (Figures 9, 12, and 13) further supports a plausible role of SIMPLE in exosomes rather than microvesicles. Hence we propose that SIMPLE mainly plays a role in exosome formation. If our model is correct, CMT1C mutation will mainly affect exosomes, and remaining

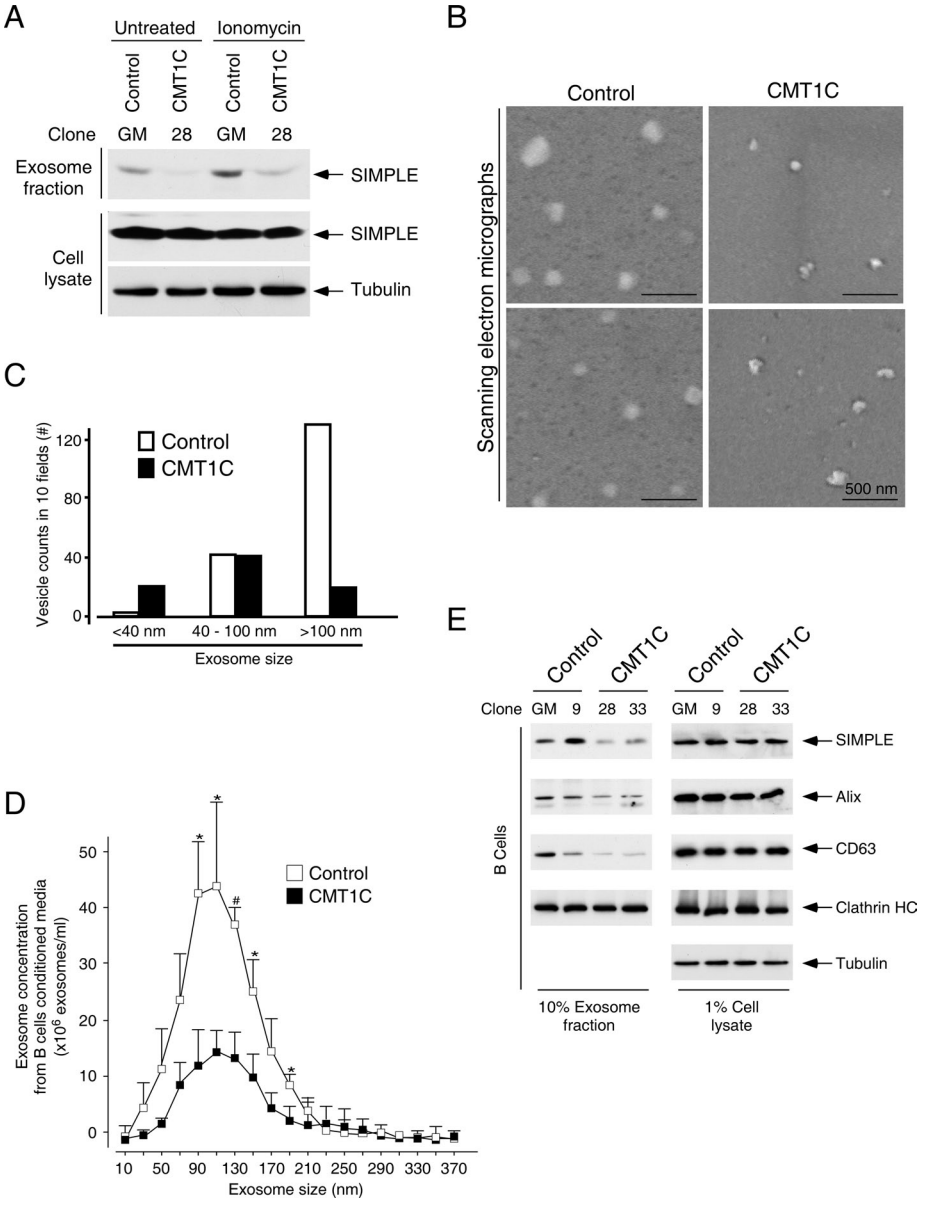

FIGURE 11: Reduced exosomal trafficking in CMT1C patient B cells. (A) The levels of endogenous SIMPLE in secreted exosomes and in cell lysates of control (clone GM) and CMT1C (clone 28) B cells were determined by immunoblotting. Effect of ionomycin is also shown. Forty percent of exosome fractions and 4% of cell lysate were examined. (B) Scanning electron microscopy was performed to reveal the appearances of exosomes secreted by control (clone GM) and CMT1C (clone 28) B cells. Representative images are shown. Scale bar, 500 nm. (C) Morphometric determination was performed to count the number and determine the size of exosomes from 10 photos taken from different fields of the EM grids. (D) Exosomes present in conditioned media of control (clone GM) and CMT1C (clone 28) B cells were quantified by nanoparticle tracking analysis. *$p < 0.05$; #$p < 0.005$. (E) Exosome proteins secreted from control and CMT1C B cells were determined by immunoblotting. Two different clones of control B cells (clones GM and 9) and two different clones of CMT1C B cells (clones 28 and 33) were examined. Ten percent of exosome fractions and 1% of cell lysate were examined.

cargoes secreted from CMT1C cells likely will be derived from microvesicles. Future proteomic assays and microarray studies to identify such proteins and RNA species secreted (or not) by CMT1C cells will provide new insights into the biochemical differences between exosomes and microvesicles. Critical biomarkers to differentiate exosomes and microvesicles may be uncovered.

Multiple signature motifs for endocytic functions are identified on SIMPLE (Figure 1). These include the di-Leu (LL) and YKRL motifs for binding of AP complexes, the PTAP motif for binding of ESCRT1 protein Tsg101, the PPxY motifs for binding of Nedd4 type E3 ubiquitin ligases, and a cluster of specific CMT1C point mutation. Our data indicate that these motifs positively and negatively contribute to the secretion of SIMPLE in exosomes (Figures 3 and 7). We surmise that proper location in the endocytic system, via protein–protein interactions with the LL, YKRL, or PTAP motifs, is critical for subsequent secretion of SIMPLE in exosomes. The PPxY motifs, however, seem to contribute a regulatory function to exosome secretion of SIMPLE. Our findings that SIMPLE encodes PTAP and PPxY regulatory motifs are in parallel with results on the arrestin domain–containing protein 1 (ARRDC1), which is mainly located on the plasma membrane (Nabhan *et al.*, 2012). Nabhan *et al.* (2012) demonstrate that ARRDC1 recruits Tsg101 and WWP2, a member of the Nedd4 type E3 ubiquitin ligases, to regulate budding of microvesicles from the plasma membrane. These findings may be related to the role of SIMPLE in regulating exosome biogenesis on the endosomal membrane. Thus future investigations to examine the regulatory role of Nedd4 type E3 ubiquitin ligases and Tsg101 in secretion of exosomes/microvesicles are warranted.

SIMPLE in CMT1C

On mutation of endogenous SIMPLE in our CMT1C model, we find reduced secretion of exosomes (Figures 8 and 11). Reduced secretion of exosomes is corroborated by the altered structures in MVBs (Figures 9, 12, and 13). In addition to the reduced concentration of exosomes, scanning electron microscopy analysis reveals that the profile of exosomes secreted was skewed, and smaller exosomes were found upon CMT1C mutation of endogenous SIMPLE (Figures 8 and 11). Quantification of exosomes using nanoparticle tracking analysis, however, only suggests a distorted trend with no obvious enrichment of smaller exosomes upon CMT1C mutation (Figures 8 and 11). Quantification of biological nanovesicles using nanoparticle tracking analysis, unfortunately, is limited to ~50 nm (Dragovic *et al.*, 2011). Thus quantification of smaller exosomes using nanoparticle tracking analysis, despite being a powerful approach to examine the overall exosome profile, may be underrepresented. Nonetheless, future studies to examine the function and interaction of SIMPLE in late endosome/MVBs, where exosomes are formed, are warranted.

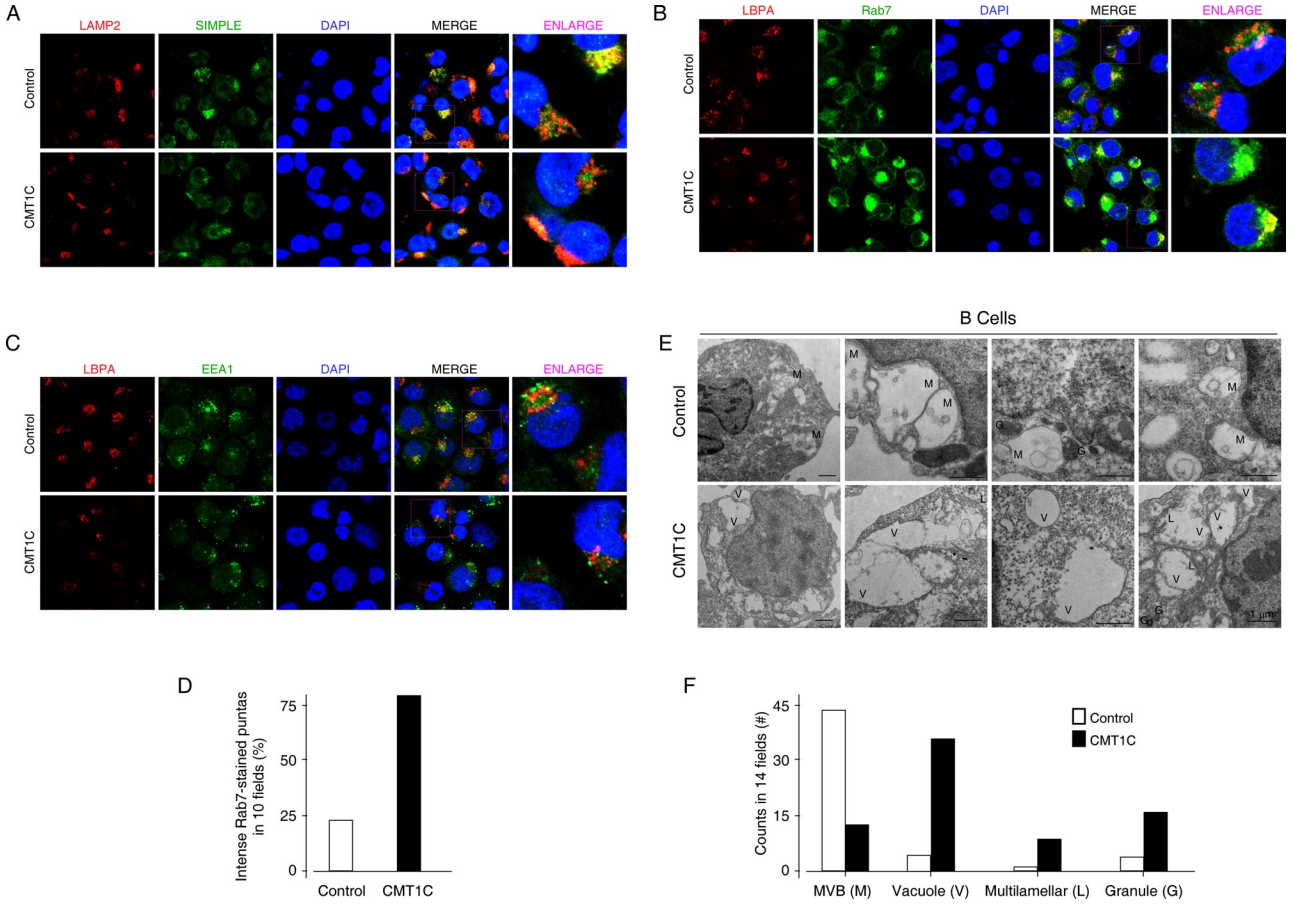

FIGURE 12: Aberrant endosomal/lysosomal compartments in CMT1C patient B cells. (A) Costaining of endogenous LAMP2 (red) and SIMPLE (green) and in control (clone GM) and CMT1C (clone 28) B cells was analyzed by confocal microscopy. DNA in nuclei was visualized using DAPI (blue). (B) Costaining of LBPA (red) and endogenous Rab7 (green) in control (clone GM) and CMT1C (clone 28) B cells. (C) Costaining of lysobisphosphatidic acid (LBPA, red) and endogenous EEA1 (green) in control (clone GM) and CMT1C (clone 28) B cells. (D) Random fields of control ($n = 8$) and CMT1C ($n = 10$) B cells were photographed, and the number of Rab7-labeled puntae was determined. (E) Transmission electron microscopy was performed to determine the ultrastructures of control (clone GM) and CMT1C (clone 28) B cells. Scale bar, 1 μm. (F) Morphometric determination was performed to count the appearances of multivesicular bodies (M), enlarged empty vacuoles (V), multilamellar cisternal compartments (L), and electron-dense granules (G) in 14 photos taken from different fields of the EM grids.

Despite the changes in appearance of endosomal/lysosomal compartments upon CMT1C mutation (Figures 9, 10, 12, and 13), we found endogenous wild-type and CMT1C-mutated SIMPLE proteins expressed to similar levels and exhibiting comparable punctated staining in MEFs and B cells (Figures 5, 6, 8, and 10–12). Subcellular fractionation of *Simple*$^{+/+}$ and *Simple*$^{T115N/+}$ MEFs further demonstrated the exclusive localization of SIMPLE in membrane fractions (Figure 6). Our observation that expression and localization of endogenous SIMPLE is unaffected by CMT1C mutation is in contrast to previous findings of mislocalization and aggregate accumulation in cells overexpressing exogenous CMT1C-mutated SIMPLE (Lee *et al.*, 2011). Indeed, we also observed similar mislocalization and aggregate accumulation of overexpressed CMT1C mutated SIMPLE (data not shown). We surmise that mislocalization and aggregate accumulation of exogenous, CMT1C-mutated SIMPLE is likely an artifact due to overexpression. Similar anomalous observations due to overexpression were found when we expressed exogenous ESCRT protein Tom1 or Hrs in cells (data not shown; Urbe *et al.*, 2000; Katoh *et al.*, 2004; Tumbarello *et al.*, 2012). Hence the peculiarity of overexpression of ESCRT machinery (or related trafficking proteins, such as SIMPLE) in limiting intracellular membranes and on endosomal trafficking warrants careful examination and data interpretation.

Changes in the appearance of endosomal/lysosomal compartments and reduced exosome biogenesis were found upon CMT1C mutation (*Simple*$^{T115N/+}$ and *Simple*$^{T115N/T115N}$) and in SIMPLE null (*Simple*$^{-/-}$; Figures 9, 10, 12, and 13 and Supplemental Figure S2). These genetic models therefore demonstrate a role of SIMPLE in late endosomes, in particular in the MVBs, and in exosome production. Morphometric determination of *Simple*$^{T115N/+}$ and *Simple*$^{-/-}$ MEFs, however, reveals distinctive malformations in the ultrastructures (Figure 9). Vacuolated appearance is evident in *Simple*$^{T115N/+}$ MEFs, whereas the presence of multilamellar cisternal compartments and accumulation of electron-dense granules are more pronounced in *Simple*$^{-/-}$ MEFs. In *Simple*$^{T115N/T115N}$ MEFs (Figure 9), electron microscopy reveals a combined phenotype with a vacuolated appearance, the presence of multilamellar cisternal compartments, and accumulation of electron-dense granules. These observations suggest that CMT1C mutation has an additional effect on the MVBs. Thus loss of expression as in SIMPLE null (*Simple*$^{-/-}$) might

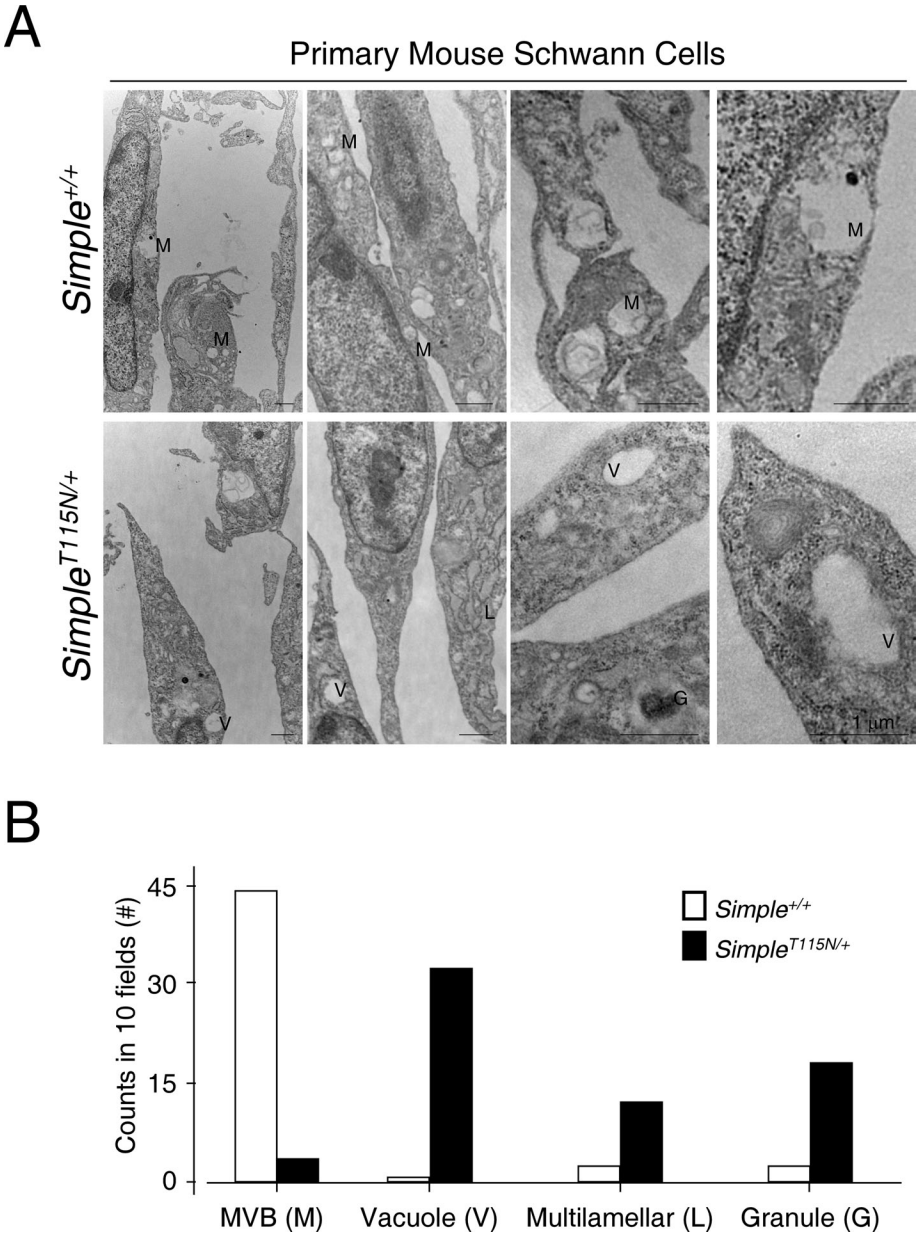

FIGURE 13: Aberrant endosomal/lysosomal compartments in CMT1C mouse primary Schwann cells. (A) Transmission electron microscopy was performed to determine the ultrastructure of *Simple*$^{+/+}$ and *Simple*$^{T115N/+}$ Schwann cells. Scale bar, 1 μm. (B) Morphometric determination was performed to count the appearances of multivesicular bodies (M), enlarged empty vacuoles (V), multilamellar cisternal compartments (L), and electron-dense granules (G) in 10 photos taken from different fields of the EM grids.

not fully recapitulate CMT1C mutation (*Simple*$^{T115N/+}$ and *Simple*$^{T115N/T115N}$). Additional gain of function might be elicited upon mutation of SIMPLE. Further biochemical characterizations of the trafficking properties and functions in *Simple*$^{T115N/+}$, *Simple*$^{-/-}$, and *Simple*$^{T115N/T115N}$ cells/mice will provide new mechanistic insights into the autosomal-dominant trait of CMT1C.

The plausible differences in the underlying mechanisms elicited by CMT1C mutation (*Simple*$^{T115N/+}$) and ablation of SIMPLE (*Simple*$^{-/-}$) were also proposed in a recent study by Somandin *et al.* (2012), who found no obvious neuropathy in *Simple*$^{-/-}$ mice even at old age (~18 mo). They surmised that the loss of SIMPLE expression could not account for neuropathy found in CMT1C patients and proposed a gain of toxic function of SIMPLE upon CMT1C mutation.

In young CMT1C mice (<12 mo), we found increased hind limb clasping (data not shown). Electrophysiological experiments to determine nerve conduction velocity, however, were indistinguishable between wild-type and CMT1C mice (data not shown), despite the aforementioned phenotype. In addition, in a cohort of ~50 mice carrying CMT1C mutations (*Simple*$^{T115N/+}$ and *Simple*$^{T115N/T115N}$ mice), we observed that ~15% of mice exhibited paralysis at old age (>18 mo; data not shown). No incidence of paralysis was found in age-matched *Simple*$^{+/+}$ or *Simple*$^{-/-}$ mice (data not shown), as reported by Somandin *et al.* (2012). Locomotor defects found in old mice, however, are difficult to interpret due to the complications of age-related factors and deteriorated heath. The low frequency of paralysis in old CMT1C mice also compounds the difficulty in obtaining compelling data with statistical significance. Perhaps, similar to the SIMPLE-null mice (Somandin *et al.*, 2012), CMT1C mice will exhibit neurological phenotypes upon challenge.

Vesicular trafficking and CMT

The role of SIMPLE in exosome production and its defects in CMT1C expand the repertoire of vesicular trafficking proteins whose mutation/deletion causes CMT diseases. Other vesicular trafficking proteins include Rab7, SH3TC2, MTMR2, MTMR13/SBF2, and FIG4, whose mutation/deletion accounts for CMT2B, CMT4C, CMT4B1, CMT4B2, and CMT4J, respectively (Senderek *et al.*, 2003a,b; Verhoeven *et al.*, 2003; Bolino *et al.*, 2004; Meggouh *et al.*, 2006; Chow *et al.*, 2007; Previtali *et al.*, 2007; Tersar *et al.*, 2007; Spinosa *et al.*, 2008; Lupo *et al.*, 2009). Similar to SIMPLE, several of these proteins, such as Rab7, MTMR2, and FIG4, are widely expressed in many different cell types to regulate vesicular trafficking. The molecular rationale for the apparent vulnerability in the peripheral nervous system in CMT diseases, however, is elusive. Future characterization of the endocytic trafficking system in axonal-myelin maintenance and Schwann cell biology is warranted.

On the other hand, although largely uncharacterized, systems other than the peripheral nervous system may be affected in CMT1C patients. In particular, SIMPLE is widely expressed in many different tissues. In addition, SIMPLE is also named LITAF for its role in immune regulation and cytokine expression in sepsis (Tang *et al.*, 2006; Srinivasan *et al.*, 2010; Merrill *et al.*, 2011). It remains elusive, however, whether CMT1C patients exhibit defects in immune regulation and function. It is hard to define pleiotropy within CMT1C patients, as there is significant clinical variability and onset even within families harboring the same mutation

(Bird, 1993; Bennett *et al.*, 2004), which further complicates this issue. Further examination of CMT1C mice and SIMPLE-null mice therefore will provide physiological relevance for the function of SIMPLE.

Reduced production of exosomes by CMT1C-mutated SIMPLE would have intracellular and extracellular pathological consequences. Dysregulated endosomal trafficking and lysosomal stress would affect intracellular homeostasis (Saksena and Emr, 2009; Stuffers *et al.*, 2009). On the other hand, reduced exosome secretion to extracellular milieu would alter intercellular communications (Thery *et al.*, 2009; Mittelbrunn and Sanchez-Madrid, 2012). Of note, either intracellular stress or ineffective extracellular communications would lead to neurological dysfunctions (Jessen and Mirsky, 2008; Taveggia *et al.*, 2010; Garden and La Spada, 2012). For example, it was shown that exosomes might play a prominent role in the propagation of α-synuclein–mediated Parkinson disease and transmission of prion proteins (Vella *et al.*, 2007; Coleman *et al.*, 2009; Emmanouilidou *et al.*, 2010; Alvarez-Erviti *et al.*, 2011; Hasegawa *et al.*, 2011; Danzer *et al.*, 2012). Future studies using *Simple*$^{T115N/+}$, *Simple*$^{-/-}$, and *Simple*$^{T115N/T115N}$ cells/mice will provide new mechanistic insights to address whether intracellular and/or extracellular consequences account for the pathological changes in CMT1C demyelination and other neurodegenerative diseases.

Conclusion

We demonstrated that SIMPLE plays a critical role in exosome formation. Mutation of SIMPLE, which abolishes the proper formation of MVBs and exosome biogenesis, could elicit intracellular and extracellular consequences and place an overwhelming burden on the nervous system, accounting for CMT1C molecular pathogenesis.

MATERIALS AND METHODS

Reagents

Polyclonal antibody against SIMPLE was generated with COOH-terminal peptide DVDHYCPNCKALLGTYKRL as antigen, using standard techniques. The primary antibodies used were SIMPLE (HPA006960; Sigma-Aldrich St. Louis, MO), LBPA (Z-SLBPA; Echelon Bioscience, Salt Lake City, UT), EEA1 (3288; Cell Signaling, Beverly, MA), Rab7 (9367; Cell Signaling), Hsp70 (SC32239; Santa Cruz Biotechnology, Santa Cruz, CA), Hsc70 (SC1059; Santa Cruz Biotechnology), Hrs (SC271925; Santa Cruz Biotechnology), Alix (611620; BD Biosciences, San Diego, CA), flotillin-1 (610820; BD Biosciences), GFP (ab5450; Abcam, Cambridge, MA), FLAG (F3165; Sigma-Aldrich St. Louis, MO), and HA (SC7392; Santa Cruz Biotechnology). CD63 (LAMP3, H5C6), LAMP1 (1D4B), LAMP2 (ABL-93), and tubulin (E7) antibodies were obtained from the monoclonal antibody facility at the University of Iowa (University Heights, IA). LactC2-RFP and LactC2-GFP were obtained from Haematologic Technologies (Essex Junction, VT). SIMPLE mutants were generated by PCR.

Mice

Animal experiments were performed in accordance with the guidelines of the Albert Einstein College of Medicine Institute of Animal Studies. A C>A point mutation was introduced into codon 115 in exon 3 of the SIMPLE gene to mutate the amino acid from Thr to Asn (T115N). A loxP (L83) site and a Frt-Neo-Frt-loxP (FNFL) cassette were then engineered to flank T115N exon 3 of the SIMPLE gene to generate the "floxed/neo" SIMPLE/T115N allele. A gene-targeting vector was constructed by retrieving the 2-kb short homology arm, 1-kb sequence containing exon 3 with T115N mutation, FNFL cassette, and 5-kb-long homology arm. The FNFL cassette conferred G418 resistance during gene targeting in PTL1 (129B6 hybrid) ES cells. Several targeted ES cells were identified and injected into C57BL/6 blastocysts to generate chimeric mice (chimeras). Male chimeras were bred to ACTB (Flpe/Flpe) females to transmit the floxed SIMPLE/T115N allele. Germline-transmitted SIMPLE/T115N mice (*Simple*$^{T115N/+}$, CMT1C mice) were mated with EIIa-Cre to delete exon 3 and generate *Simple*$^{-/+}$ mice. *Simple*$^{T115N/+}$ and *Simple*$^{-/+}$ mice were backcrossed into C57BL/6 at least six times before use.

Cell culture

Primary mouse embryonic fibroblasts with genotypes of *Simple*$^{+/+}$, *Simple*$^{T115N/+}$, *Simple*$^{T115N/T115N}$, and *Simple*$^{-/-}$ were isolated from E13.5 pups and cultured as described previously (Yang *et al.*, 2006). Primary mouse Schwann cells were isolated from dorsal root ganglia of E13.5 pups and cultured as described previously (Yang *et al.*, 2012). Primary rat Schwann cells and EBV-transformed B cells were cultured as described previously (Shirk *et al.*, 2005; Maurel *et al.*, 2007). Two different clones of control B cells (clones GM and 9) and two different clones of CMT1C B cells (clones 28 and 33) were examined. COS cells and HepG2 cells were cultured in DMEM and MEM, respectively. Transient transfections on COS and HepG2 cells were carried out using Lipofectamine (Invitrogen, Carlsbad, CA) according to the manufacturer. All media were supplemented with 10% fetal calf serum, 2 mM L-glutamine, penicillin (100 U/ml), and streptomycin (100 μg/ml; Invitrogen). Cells were transfected by using Lipofectamine.

Confocal microscopy

Cells were plated on coverslips 24 h before the experiment. Cells were washed three times in cold PBS and fixed in 4% paraformaldehyde for 15 min. For staining of LBPA, cells were fixed and permeabilized in 3.7% (wt/vol) PFA and 0.1% glutaraldehyde in 0.15 mg/ml saponin solution prepared in fixative buffer (5 mM KCl, 137 mM NaCl, 4 mM $NaHCO_3$, 0.4 mM KH_2PO_4, 1.1 mM Na_2HPO_4, 2 mM $MgCl_2$, 5 mM 1,4-piperazinediethanesulfonic acid, pH 7.2, 2 mM ethylene glycol tetraacetic acid, and 5.5 mM glucose) for 40 min at 37°C. Paraformaldehyde was quenched by 0.1 M glycine in PBS for 10 min. After incubation in blocking solution (0.5% bovine serum albumin [BSA], 0.1% saponin, and 1% fetal bovine serum in PBS) the cells were incubated with primary antibodies at 4°C overnight, followed by secondary antibodies for 1 h at room temperature. All images were taken with a Leica AOBS SP2 confocal microscope (Leica, Wetzlar, Germany) with a 63× objective lens; primary representative images are shown.

Electron microscopy

Cells were fixed in a mixture of 2.5% glutaraldehyde and 4% paraformaldehyde in PBS for 2.5 h at room temperature (RT). After rinsing six times in PBS, cells were postfixed in 4% uranyl acetate at RT overnight and 1% osmium tetraoxide in PBS for 1 h at RT. Fixed cells were left in 70% ethanol overnight at 4°C and subjected to dehydration with ethanol. Once dehydrated, cells were transitioned twice with propylene oxide and then left in a 1:1 mixture of propylene oxide with Spurr's resin overnight at RT. After embedding and polymerization in Spurr's resin, 70-nm ultrathin sections were made on a Leica Ultracut Ultramicrotome (Leica Microsystems, Buffalo Grove, IL), and sections were collected on 200-mesh copper grids. Sections were poststained with 4% uranyl acetate for 60 min, rinsed, and examined with a FEI Tecnai G2 Twin Spirit Transmission electron microscope (FEI, Hillsboro, OR) operated at 80 kV. Digital images were obtained using an AMT digital camera (AMT, Woburn, MA). For

immuno–electron microscopy, cells were prepared as described, and sections were collected on nickel grids. Grids were submerged in beakers filled with 95°C sodium citrate buffer, pH 6.0, for 12.5 min. After cooling, grids were blocked in a mixture of 1% BSA with 10% goat serum in PBS at RT for 1 h. Grids were then incubated with primary antibody and secondary antibody conjugated with a 10-nm gold particles (Electron Microscopy Sciences, Hatfield, PA). Grids were rinsed and stained with 4% uranyl acetate for 1 h. Grids for immuno–electron microscopy were examined and imaged as described. For scanning electron microscopy to visualize exosomes, concentrated exosome fractions were resuspended in PBS and spotted onto polylysine-coated coverslips. After adsorption at RT for 40 min, coverslips were fixed with a mixture of 2.5% glutaraldehyde and 4% paraformaldehyde in PBS for 5 min. Coverslips were then rinsed with water and left to air dry overnight. Coverslips were then mounted onto an aluminum specimen stub and coated with gold. Exosomes were examined in an Amray 1910 Field Emission Scanning Electron Microscope operated between 5 and 7 kV (Amray, Bedford, MA). For immuno-electron microscopy labeling of exosomes, exosomes were absorbed into the grid as described. Grids were blocked in a mixture of 1% BSA with 10% goat serum and 0.4% Triton X-100 in PBS for 60 min before incubation with primary antibody at 4°C overnight. After rinses, grids were labeled with secondary antibody conjugated with 2-nm gold particles and silver enhanced using R-Gent SE-EM (Electron Microscopy Sciences). Exosomes were stained for 1 h using 4% uranyl acetate and examined as described. Morphometric determination of the ultrastructures was carried out by counting the appearances of MVBs, vacuoles, multilamellar cisternal compartments, and granules in at least 10 different photographs obtained from distinct sections of electron microscope (EM) grids. Similar morphometric determination was carried out to count the number and measure the size of exosomes in multiple EM photographs. The sum of each phenotype from counting multiple EM photographs is presented.

Exosome analysis

Conditioned media collected from cell culture supernatants were centrifuged at 1000 × *g* for 10 min and 10,000 × *g* for 40 min. The supernatant from the final centrifugation was subjected to ultracentrifugation at 100,000 × *g* for 1 h to isolate exosome pellet. Exosome pellet was resuspended in 0.25 M sucrose solution for ultracentrifugation in 0.25–2.5 M sucrose density gradient as described previously (Trajkovic *et al.*, 2008). For immunoprecipitation assays, exosome pellet was resuspended in either PBS or Triton-lysis buffer (20 mM Tris, pH 7.4, 134 mM NaCl, 2 mM EDTA, 25 mM β-glycerophosphate, 2 mM NaPPi, 10% glycerol, 1% Triton X-100, 1 mM phenylmethylsulfonyl fluoride, 1 mM benzamidine, and 10 µg/ml leupeptin) and subjected to immunoprecipitation using SIMPLE antibodies. For limited trypsin digest, exosome pellet was digested in 0.1% trypsin solution for 8 min at 37°C. For Western blotting, exosome pellet was resuspended in 1× Laemmli buffer and separated by SDS–PAGE for immunoblot analysis. For quantification of exosomes using LactC2-RFP reporter in transfected cells, cells were cotransfected with 0.2 µg of LactC2-RFP and varied amount of SIMPLE constructs (0.2–1 µg). After transfection, culture medium was replaced with phenol red–free DMEM to collect exosomes for 24 h. Collected medium were spun at 1000 × *g* for 5 min and then 10,000 × *g* for 40 min to remove cell debris. Isolated supernatant (200 µl) was transferred to a 96-well black-bottom plate. RFP signals in the isolated supernatant were detected by SpectraMax M5 microplate reader (Molecular Devices, Sunnyvale, CA) with excitation and emission at 517 and 610 nm, respectively. For nanoparticle tracking analysis, harvested exosomes were resuspended in PBS, and the concentration of exosomes was determined by using the LM10 nanoparticle characterization system (NanoSight, Amesbury, United Kingdom) equipped with a blue laser (405 nm). Parameters for the settings on NanoSight were as follows: shutter, 500; gain, 256; capture, 60 s; threshold, 13; minimum expected particle size, 30 nm.

ACKNOWLEDGMENTS

We thank members of our laboratories for their suggestions and critical reading of the manuscript. We are grateful for the generosity of Phillip Chance in providing reagents and critical reading of the manuscript. We also thank Mercedes Rincon and Tony Ip for support and comments on the manuscript. This research is supported, in part, by grants from the Muscular Dystrophy Association (C.-W.C.).

REFERENCES

Alvarez-Erviti L, Seow Y, Schapira AH, Gardiner C, Sargent IL, Wood MJ, Cooper JM (2011). Lysosomal dysfunction increases exosome-mediated alpha-synuclein release and transmission. Neurobiol Dis 42, 360–367.

Aoki N, Jin-No S, Nakagawa Y, Asai N, Arakawa E, Tamura N, Tamura T, Matsuda T (2007). Identification and characterization of microvesicles secreted by 3T3-L1 adipocytes: redox- and hormone-dependent induction of MFG-E8-associated microvesicles. Endocrinology 148, 3850–3862.

Bennett CL *et al.* (2004). SIMPLE mutation in demyelinating neuropathy and distribution in sciatic nerve. Ann Neurol 55, 713–720.

Bird TD (1993). Charcot-Marie-Tooth neuropathy type 1. In: GeneReviews, ed. RA Pagon, TD Bird, CR Dolan, K Stephens, and MP Adam, Seattle, WA: University of Washington.

Boerkoel CF *et al.* (2002). Charcot-Marie-Tooth disease and related neuropathies: mutation distribution and genotype-phenotype correlation. Ann Neurol 51, 190–201.

Bolcato-Bellemin AL, Mattei MG, Fenton M, Amar S (2004). Molecular cloning and characterization of mouse LITAF cDNA: role in the regulation of tumor necrosis factor-alpha (TNF-alpha) gene expression. J Endotoxin Res 10, 15–23.

Bolino A *et al.* (2004). Disruption of Mtmr2 produces CMT4B1-like neuropathy with myelin outfolding and impaired spermatogenesis. J Cell Biol 167, 711–721.

Bonifacino JS, Traub LM (2003). Signals for sorting of transmembrane proteins to endosomes and lysosomes. Annu Rev Biochem 72, 395–447.

Chaput N *et al.* (2006). Dendritic cell derived-exosomes: biology and clinical implementations. J Leukoc Biol 80, 471–478.

Chen C, Matesic LE (2007). The Nedd4-like family of E3 ubiquitin ligases and cancer. Cancer Metastasis Rev 26, 587–604.

Chow CY *et al.* (2007). Mutation of FIG4 causes neurodegeneration in the pale tremor mouse and patients with CMT4J. Nature 448, 68–72.

Coleman BM, Nisbet RM, Han S, Cappai R, Hatters DM, Hill AF (2009). Conformational detection of prion protein with biarsenical labeling and FlAsH fluorescence. Biochem Biophys Res Commun 380, 564–568.

Danzer KM, Kranich LR, Ruf WP, Cagsal-Getkin O, Winslow AR, Zhu L, Vanderburg CR, McLean PJ (2012). Exosomal cell-to-cell transmission of alpha synuclein oligomers. Mol Neurodegener 7, 42.

de Gassart A, Geminard C, Fevrier B, Raposo G, Vidal M (2003). Lipid raft-associated protein sorting in exosomes. Blood 102, 4336–4344.

Dragovic *et al.* (2011). Sizing and phenotyping of cellular vesicles using nanoparticle tracking analysis. Nanomedicine 7, 780–788.

Eaton HE, Desrochers G, Drory SB, Metcalf J, Angers A, Brunetti CR (2011). SIMPLE/LITAF expression induces the translocation of the ubiquitin ligase itch towards the lysosomal compartments. PLoS One 6, e16873.

Emmanouilidou E, Melachroinou K, Roumeliotis T, Garbis SD, Ntzouni M, Margaritis LH, Stefanis L, Vekrellis K (2010). Cell-produced alpha-synuclein is secreted in a calcium-dependent manner by exosomes and impacts neuronal survival. J Neurosci 30, 6838–6851.

Falguières T, P-Luyet P, Gruenberg J (2009). Molecular assemblies and membrane domains in multivesicular endosome dynamics. Exp Cell Res 315, 1567–1573.

Fang Y, Wu N, Gan X, Yan W, Morrell JC, Gould SJ (2007). Higher-order oligomerization targets plasma membrane proteins and HIV gag to exosomes. PLoS Biol 5, e158.

Felberbaum-Corti M, Cavalli V, Gruenberg J (2005). Capture of the small GTPase Rab5 by GDI: regulation by p38 MAP kinase. Methods Enzymol 403, 367–381.
Garden GA, La Spada AR (2012). Intercellular (mis)communication in neurodegenerative disease. Neuron 73, 886–901.
Gerding WM, Koetting J, Epplen JT, Neusch C (2009). Hereditary motor and sensory neuropathy caused by a novel mutation in LITAF. Neuromuscul Disord 19, 701–703.
Giri PK, Kruh NA, Dobos KM, Schorey JS (2010). Proteomic analysis identifies highly antigenic proteins in exosomes from *M. tuberculosis*-infected and culture filtrate protein-treated macrophages. Proteomics 10, 3190–3202.
Giri PK, Schorey JS (2008). Exosomes derived from *M. bovis* BCG infected macrophages activate antigen-specific CD4+ and CD8+ T cells in vitro and in vivo. PLoS One 3, e2461.
Haglund K, Dikic I (2005). Ubiquitylation and cell signaling. EMBO J 24, 3353–3359.
Hasegawa T *et al.* (2011). The AAA-ATPase VPS4 regulates extracellular secretion and lysosomal targeting of alpha-synuclein. PLoS One 6, e29460.
Henne WM, Buchkovich NJ, Emr SD (2011). The ESCRT pathway. Dev Cell 21, 77–91.
Huang Y, Bennett CL (2007). Litaf/Simple protein is increased in intestinal tissues from patients with CD and UC, but is unlikely to function as a transcription factor. Inflamm Bowel Dis 13, 120–121.
Huotari J, Helenius A (2011). Endosome maturation. EMBO J 30, 3481–3500.
Hurley JH (2010). The ESCRT complexes. Crit Rev Biochem Mol Biol 45, 463–487.
Hurley JH, Boura E, Carlson LA, Rozycki B (2011). Membrane budding. Cell 143, 875–887.
Hurley JH, Emr SD (2006). The ESCRT Complexes: structure and mechanism of a membrane-trafficking network. Annu Rev Biophys Biomol Struct 35, 277–298.
Hurley JH, Hanson PI (2010). Membrane budding and scission by the ESCRT machinery: it's all in the neck. Nat Rev Mol Cell Biol 11, 556–566.
Jessen KR, Mirsky R (2008). Negative regulation of myelination: relevance for development, injury, and demyelinating disease. Glia 56, 1552–1565.
Jolliffe CN, Harvey KF, Haines BP, Parasivam G, Kumar S (2000). Identification of multiple proteins expressed in murine embryos as binding partners for the WW domains of the ubiquitin-protein ligase Nedd4. Biochem J 351 Pt 3, 557–565.
Katoh Y, Shiba Y, Mitsuhashi H, Yanagida Y, Takatsu H, Nakayama K (2004). Tollip and Tom1 form a complex and recruit ubiquitin-conjugated proteins onto early endosomes. J Biol Chem 279, 24435–24443.
Kramer-Albers EM, Bretz N, Tenzer S, Winterstein C, Mobius W, Berger H, Nave KA, Schild H, Trotter J (2007). Oligodendrocytes secrete exosomes containing major myelin and stress-protective proteins: trophic support for axons? Proteomics Clin Appl 1, 1446–1461.
Latour P *et al.* (2006). SIMPLE mutation analysis in dominant demyelinating Charcot-Marie-Tooth disease: three novel mutations. J Peripher Nerv Syst 11, 148–155.
Lee SM, Olzmann JA, Chin LS, Li L (2011). Mutations associated with Charcot-Marie-Tooth disease cause SIMPLE protein mislocalization and degradation by the proteasome and aggresome-autophagy pathways. J Cell Sci 124, 3319–3331.
Li XB, Zhang ZR, Schluesener HJ, Xu SQ (2006). Role of exosomes in immune regulation. J Cell Mol Med 10, 364–375.
Lupo V, Galindo MI, Martinez-Rubio D, Sevilla T, Vilchez JJ, Palau F, Espinos C (2009). Missense mutations in the SH3TC2 protein causing Charcot-Marie-Tooth disease type 4C affect its localization in the plasma membrane and endocytic pathway. Hum Mol Genet 18, 4603–4614.
Mathivanan S, Simpson RJ (2009). ExoCarta: a compendium of exosomal proteins and RNA. Proteomics 9, 4997–5000.
Maurel P, Einheber S, Galinska J, Thaker P, Lam I, Rubin MB, Scherer SS, Murakami Y, Gutmann DH, Salzer JL (2007). Nectin-like proteins mediate axon Schwann cell interactions along the internode and are essential for myelination. J Cell Biol 178, 861–874.
Meggouh F, Bienfait HM, Weterman MA, de Visser M, Baas F (2006). Charcot-Marie-Tooth disease due to a de novo mutation of the RAB7 gene. Neurology 67, 1476–1478.
Merrill JC, You J, Constable C, Leeman SE, Amar S (2011). Whole-body deletion of LPS-induced TNF-alpha factor (LITAF) markedly improves experimental endotoxic shock and inflammatory arthritis. Proc Natl Acad Sci USA 108, 21247–21252.
Mignot G, Roux S, Thery C, Segura E, Zitvogel L (2006). Prospects for exosomes in immunotherapy of cancer. J Cell Mol Med 10, 376–388.
Mittelbrunn M, Gutierrez-Vazquez C, Villarroya-Beltri C, Gonzalez S, Sanchez-Cabo F, Gonzalez MA, Bernad A, Sanchez-Madrid F (2011). Unidirectional transfer of microRNA-loaded exosomes from T cells to antigen-presenting cells. Nat Commun 2, 282.
Mittelbrunn M, Sanchez-Madrid F (2012). Intercellular communication: diverse structures for exchange of genetic information. Nat Rev Mol Cell Biol 13, 328–335.
Morita E, Sundquist W (2004). Retrovirus budding. Annu Rev Cell Dev Biol 20, 395.
Moriwaki Y, Begum NA, Kobayashi M, Matsumoto M, Toyoshima K, Seya T (2001). *Mycobacterium bovis* bacillus Calmette-Guerin and its cell wall complex induce a novel lysosomal membrane protein, SIMPLE, that bridges the missing link between lipopolysaccharide and p53-inducible gene, LITAF(PIG7), and estrogen-inducible gene, EET-1. J Biol Chem 276, 23065–23076.
Myokai F, Takashiba S, Lebo R, Amar S (1999). A novel lipopolysaccharide-induced transcription factor regulating tumor necrosis factor alpha gene expression: molecular cloning, sequencing, characterization, and chromosomal assignment. Proc Natl Acad Sci USA 96, 4518–4523.
Nabhan JF, Hu R, Oh RS, Cohen SN, Lu Q (2012). Formation and release of arrestin domain-containing protein 1-mediated microvesicles (ARMMs) at plasma membrane by recruitment of TSG101 protein. Proc Natl Acad Sci USA 109, 4146–4151.
Natesan S, Rivera VM, Molinari E, Gilman M (1997). Transcriptional squelching re-examined. Nature 390, 349–350.
Piper R, Katzmann D (2007). Biogenesis and function of multivesicular bodies. Annu Rev Cell Dev Biol 23, 519.
Previtali SC, Quattrini A, Bolino A (2007). Charcot-Marie-Tooth type 4B demyelinating neuropathy: deciphering the role of MTMR phosphatases. Expert Rev Mol Med 9, 1–16.
Rauch S, Martin-Serrano J (2011). Multiple interactions between the ESCRT machinery and arrestin-related proteins: implications for PPXY-dependent budding. J Virol 85, 3546–3556.
Raymond CK, Howald-Stevenson I, Vater CA, Stevens TH (1992). Morphological classification of the yeast vacuolar protein sorting mutants: evidence for a prevacuolar compartment in class E vps mutants. Mol Biol Cell 3, 1389–1402.
Rieder SE, Banta LM, Kohrer K, McCaffery JM, Emr SD (1996). Multilamellar endosome-like compartment accumulates in the yeast vps28 vacuolar protein sorting mutant. Mol Biol Cell 7, 985–999.
Rusten TE, Vaccari T, Stenmark H (2012). Shaping development with ESCRTs. Nat Cell Biol 14, 38–45.
Saifi GM *et al.* (2005). SIMPLE mutations in Charcot-Marie-Tooth disease and the potential role of its protein product in protein degradation. Hum Mutat 25, 372–383.
Saksena S, Emr SD (2009). ESCRTs and human disease. Biochem Soc Trans 37, 167–172.
Schartz NE, Chaput N, Andre F, Zitvogel L (2002). From the antigen-presenting cell to the antigen-presenting vesicle: the exosomes. Curr Opin Mol Ther 4, 372–381.
Senderek J *et al.* (2003a). Mutations in a gene encoding a novel SH3/TPR domain protein cause autosomal recessive Charcot-Marie-Tooth type 4C neuropathy. Am J Hum Genet 73, 1106–1119.
Senderek J, Bergmann C, Weber S, Ketelsen UP, Schorle H, Rudnik-Schoneborn S, Buttner R, Buchheim E, Zerres K (2003b). Mutation of the SBF2 gene, encoding a novel member of the myotubularin family, in Charcot-Marie-Tooth neuropathy type 4B2/11p15. Hum Mol Genet 12, 349–356.
Shirk AJ, Anderson SK, Hashemi SH, Chance PF, Bennett CL (2005). SIMPLE interacts with NEDD4 and TSG101: evidence for a role in lysosomal sorting and implications for Charcot-Marie-Tooth disease. J Neurosci Res 82, 43–50.
Shy ME (2004). Charcot-Marie-Tooth disease: an update. Curr Opin Neurol 17, 579–585.
Simons M, Raposo G (2009). Exosomes—vesicular carriers for intercellular communication. Curr Opin Cell Biol 21, 575–581.
Simpson RJ, Jensen SS, Lim JWE (2008). Proteomic profiling of exosomes: current perspectives. Proteomics 8, 4083–4099.
Slagsvold T, Pattni K, Malerod L, Stenmark H (2006). Endosomal and non-endosomal functions of ESCRT proteins. Trends Cell Biol 16, 317–326.
Somandin C, Gerber D, Pereira JA, Horn M, Suter U (2012). LITAF (SIMPLE) regulates Wallerian degeneration after injury but is not essential for

peripheral nerve development and maintenance: implications for Charcot-Marie-Tooth disease. Glia 60, 1518–1528.
Spinosa MR, Progida C, De Luca A, Colucci AM, Alifano P, Bucci C (2008). Functional characterization of Rab7 mutant proteins associated with Charcot-Marie-Tooth type 2B disease. J Neurosci 28, 1640–1648.
Srinivasan S, Leeman SE, Amar S (2010). Beneficial dysregulation of the time course of inflammatory mediators in lipopolysaccharide-induced tumor necrosis factor alpha factor-deficient mice. Clin Vaccine Immunol 17, 699–704.
Street VA, Bennett CL, Goldy JD, Shirk AJ, Kleopa KA, Tempel BL, Lipe HP, Scherer SS, Bird TD, Chance PF (2003). Mutation of a putative protein degradation gene LITAF/SIMPLE in Charcot-Marie-Tooth disease 1C. Neurology 60, 22–26.
Stuffers S, Brech A, Stenmark H (2009). ESCRT proteins in physiology and disease. Exp Cell Res 315, 1619–1626.
Szigeti K, Lupski JR (2009). Charcot-Marie-Tooth disease. Eur J Hum Genet 17, 703–710.
Tang X, Marciano DL, Leeman SE, Amar S (2005). LPS induces the interaction of a transcription factor, LPS-induced TNF-alpha factor, and STAT6(B) with effects on multiple cytokines. Proc Natl Acad Sci USA 102, 5132–5137.
Tang X, Metzger D, Leeman S, Amar S (2006). LPS-induced TNF-alpha factor (LITAF)-deficient mice express reduced LPS-induced cytokine: evidence for LITAF-dependent LPS signaling pathways. Proc Natl Acad Sci USA 103, 13777–13782.
Taveggia C, Feltri ML, Wrabetz L (2010). Signals to promote myelin formation and repair. Nat Rev Neurol 6, 276–287.
Tersar K, Boentert M, Berger P, Bonneick S, Wessig C, Toyka KV, Young P, Suter U (2007). Mtmr13/Sbf2-deficient mice: an animal model for CMT4B2. Hum Mol Genet 16, 2991–3001.
Thery C, Ostrowski M, Segura E (2009). Membrane vesicles as conveyors of immune responses. Nat Rev Immunol 9, 581–593.
Timmins J, Schoehn G, Ricard-Blum S, Scianimanico S, Vernet T, Ruigrok RW, Weissenhorn W (2003). Ebola virus matrix protein VP40 interaction with human cellular factors Tsg101 and Nedd4. J Mol Biol 326, 493–502.
Trajkovic K, Hsu C, Chiantia S, Rajendran L, Wenzel D, Wieland F, Schwille P, Brugger B, Simons M (2008). Ceramide triggers budding of exosome vesicles into multivesicular endosomes. Science 319, 1244–1247.
Tumbarello DA, Waxse BJ, Arden SD, Bright NA, Kendrick-Jones J, Buss F (2012). Autophagy receptors link myosin VI to autophagosomes to mediate Tom1-dependent autophagosome maturation and fusion with the lysosome. Nat Cell Biol 14, 1024–1035.
Urbe S, Mills IG, Stenmark H, Kitamura N, Clague MJ (2000). Endosomal localization and receptor dynamics determine tyrosine phosphorylation of hepatocyte growth factor-regulated tyrosine kinase substrate. Mol Cell Biol 20, 7685–7692.
van Niel G, Porto-Carreiro I, Simoes S, Raposo G (2006). Exosomes: a common pathway for a specialized function. J Biochem 140, 13–21.
Vella LJ, Sharples RA, Lawson VA, Masters CL, Cappai R, Hill AF (2007). Packaging of prions into exosomes is associated with a novel pathway of PrP processing. J Pathol 211, 582–590.
Verhoeven K *et al.* (2003). Mutations in the small GTP-ase late endosomal protein RAB7 cause Charcot-Marie-Tooth type 2B neuropathy. Am J Hum Genet 72, 722–727.
Wang T, Ming Z, Xiaochun W, Hong W (2011). Rab7: role of its protein interaction cascades in endo-lysosomal traffic. Cell Signal 23, 516–521.
Xie LP, Fu WX, Jin C, Dong XY, Chen WF (2002). Negative regulation of monocyte chemoattractant protein-1 gene expression by a mouse estrogen-enhanced transcript. Eur J Immunol 32, 2837–2846.
Yang DP *et al.* (2012). p38 MAPK activation promotes denervated Schwann cell phenotype and functions as a negative regulator of Schwann cell differentiation and myelination. J Neurosci 32, 7158–7168.
Yang TT *et al.* (2006). Role of transcription factor NFAT in glucose and insulin homeostasis. Mol Cell Biol 26, 7372–7387.
Yeung T, Gilbert GE, Shi J, Silvius J, Kapus A, Grinstein S (2008). Membrane phosphatidylserine regulates surface charge and protein localization. Science 319, 210–213.
Zhu J, Jiang J, Zhou W, Zhu K, Chen X (1999). Differential regulation of cellular target genes by p53 devoid of the PXXP motifs with impaired apoptotic activity. Oncogene 18, 2149–2155.
Zwang Y, Yarden Y (2009). Systems biology of growth factor-induced receptor endocytosis. Traffic 10, 349–363.